

HU ISSN 1785-6892 in print
HU ISSN 2064-7522 online

DESIGN OF MACHINES AND STRUCTURES

A Publication of the University of Miskolc

Volume 8, Number 1



Miskolc University Press
2018

EDITORIAL BOARD

- Á. DÖBRÖCZÖNI
Editor in Chief
Institute of Machine and Product Design
University of Miskolc
H-3515 Miskolc-Egyetemváros, Hungary
machda@uni-miskolc.hu
- Á. TAKÁCS
Assistant Editor
Institute of Machine and Product Design
University of Miskolc
H-3515 Miskolc-Egyetemváros, Hungary
takacs.agnes@uni-miskolc.hu
- R. CERMAK
Department of Machine Design
University of West Bohemia
Univerzitni 8, 30614 Plzen, Czech Republic
rcermak@kks.zcu.cz
- B. M. SHCHOKIN
Consultant at Magna International Toronto
borys.shchokin@sympatico.ca
- W. EICHLSEDER
Institut für Allgemeinen Maschinenbau
Montanuniversität Leoben,
Franz-Josef Str. 18, 8700 Leoben, Österreich
wilfrid.eichlseder@notes.unileoben.ac.at
- S. VAJNA
Institut für Maschinenkonstruktion,
Otto-von-Guericke-Universität Magdeburg,
Universität Platz 2, 39106 MAGDEBURG, Deutschland
vajna@mb.uni-magdeburg.de
- P. HORÁK
Department of Machine and Product Design
Budapest University of Technology and Economics
horak.peter@gt3.bme.hu
H-1111 Budapest, Műegyetem rkp. 9.
MG. ép. I. em. 5.
- K. JÁRMAI
Institute of Materials Handling and Logistics
University of Miskolc
H-3515 Miskolc-Egyetemváros, Hungary
altjar@uni-miskolc.hu
- L. KAMONDI
Institute of Machine and Product Design
University of Miskolc
H-3515 Miskolc-Egyetemváros, Hungary
machkl@uni-miskolc.hu
- GY. PATKÓ
Department of Machine Tools
University of Miskolc
H-3515 Miskolc-Egyetemváros, Hungary
patko@uni-miskolc.hu
- J. PÉTER
Institute of Machine and Product Design
University of Miskolc
H-3515 Miskolc-Egyetemváros, Hungary
machpj@uni-miskolc.hu

CONTENTS

<i>Lajos, Bence Balázs–Kelemen, László: Designing pneumatic circuit of a cheese slicer</i>	5
<i>Németh, Géza: Friction assessment of lubricated steel surfaces I</i>	18
<i>Sipkás, Vivien–Bognár, Gabriella: Micro switch failure analysis</i>	29
<i>Szávai, Szabolcs–Kovács, Sándor: Implementation of a shell like thermo elasto-hydrodynamic contact element to a commercial FEM software</i>	36
<i>Tóth, Dániel–Szilágyi, Attila–Takács, György: Methods for the detection and analysis of bearing failures</i>	45
<i>Tóth, Sándor Gergő–Takács, György–Szilágyi, Attila: Current development focuses of the hydrostatic bearing design and optimization</i>	52

DESIGNING PNEUMATIC CIRCUIT OF A CHEESE SLICER

BENCE BALÁZS LAJOS–LÁSZLÓ KELEMEN

University of Miskolc, Department of Machine and Product Design
3515 Miskolc-Egyetemváros
lbence101010@gmail.com

Abstract: The design of the cheese cutter system was the one of the project topics in the HEIBUS project in 2017. My task was the design of the pneumatic system, which is used by the machine. I made the easiest solving, which complete the demands, which the design stands up. After then I sizing the main part of the circuit, and choose the other parts. I make some test in final elements program.

Keywords: *cheese cutter, pneumatic system, design, sizing*

1. INTRODUCTION

In 2017, the HEIBus organized two; international project works in Europe between three country's universities. One of these projects is a design of a cheese cutter machine and this project attended a Romanian, a German and a Hungarian university, the University of Miskolc. We got this task from the AutoMates Company, which products special machines for the industry, in this case for the food industry. A student team has six members, two students from all three universities. From the three team two took apart an intensive week in Cluj-Napoca, and one of team follow the presentations of the intensive week online. On this week the students and the mentor professors visited presentation about the Company, the task and the technical solutions which will be useful for the project.

As I wrote, the task was given by the AutoMates Company, and this company given some points, which we had to take into the account in the designing process. This point is connecting to the demands of the food industry, especially the dairy industry. In their presentation showed the demands and the suggestions.

Some points from the demands:

- full pneumatic system
- easy cleanable parts
- non-electric part
- easy transportable construction
- use Festo's pneumatic parts

In the dairy industry the speed and well organized production process are very important because of the easy perishability [1]. One of the main demands is the full

pneumatic system. In food industry the pneumatic system is the best driving solution, because it clean, the “fuel” is not pollutes the environment and the productions. The working elements have simply structure, and because of it this parts are relatively cheaper, than another method.

The pneumatic system has some bad point. For example, the air needs preparations. The “fuel” does not contain contaminations or water, because these cause the shorter lifetime of the circuit parts. This preparation and air compression for the right working pressure value is expensive. The air is squeezable, so we cannot use for precise positioning [2].

Another point is the easy cleanable and stainless parts. It’s important, mainly in the dairy products. So, we have to design the parts from plastic, stainless steel and another material, which are compatible with the food industry [3].

The wet and damp environment requires the non-electronic parts in the pneumatic system. The construction have to be simple, and easy packable, because the machine manufacture want easy transportation between the manufacture and the food industry. The main part of the designing was the collecting the ideas for the problem solving. The project stands the main demands, and we made the ideas. We, the team discuss idea and we selected the best one, which solve the problem and optimize the system, and costs. It was not easy, because often the best one was the most expensive.

2. THE PNEUMATIC CIRCUIT

The *Figure 1* shows the basic pneumatic circuit of the machine.

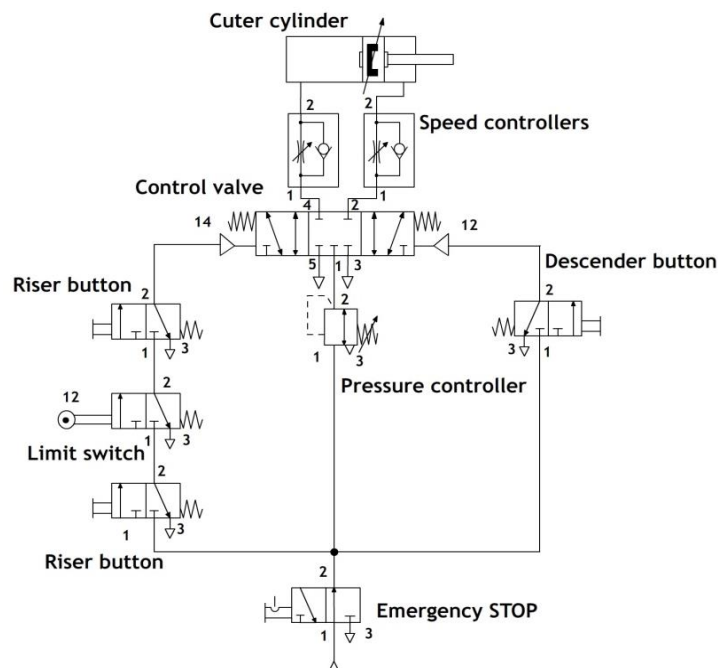


Figure 1. The pneumatic circuit in progress

One cylinder and these cylinders push up the cheese, which is on the plate, through the blades' frame. The plate has trenches, for the blades to do the full cutting, like the French fries maker. We choose this plan, because, in our opinion, this is the less expensive system. The size of the machine is significantly reduced with this circuit. The cylinder stands vertical, and the height of the cheese is smaller than the other parameter, so we do not need long stroke length. This layout causes gravity to help keep the position of the cheese on the plate. The sketch is in *Figure 2*. This sketch includes the main construction and the main movements.

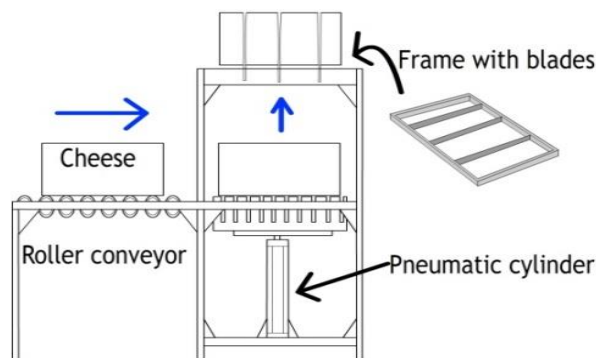


Figure 2. The best idea's sketch

2.1. Working

The preparation unit is not on the plan, but in the design process, I choose it, and it includes the main parts of a preparation unit, like the filter, the humid condenser, oiler and manometer.

The *cutter cylinder* goes out to the outer limit position, if the operator pushes simultaneously the two *riser buttons* and the *limit switch*. The limit switch is built in the door of the cutter chamber. If the switch is active, this indicates the door is closed.

If the worker opens the door, the controlling valve goes back to central position and the cylinder stops. This action activates the *5/3 control valve*, and the working pressure can flow through it, and push the cylinder out. The *riser buttons* are connected each other in *AND* logic, so the mechanism is working just we push the buttons. The *riser buttons* are *3/2-es* directional, mono stable valve, with spring returning.

The *5/3* directional valve central state is closed state, so when both sides are active, the valve is closed, and the cylinder holds the position. We can use this function to positioning between the two limit positions, but it is not accurate, because the air is squeezable.

After the *5/3* valve, – in the pneumatic line – is *the speed controllers*. With this one way flow control valve the worker can set the speed of the cylinder movement. This valve sets just the outgoing speed.

Then the cutting is over, the worker can set the cylinder in the starter position, after he or she take off the cut parts of the cheese, if he or she pushes the *descender*

button. This valve activates the 5/3 valve for the other ending position. This causes the reverse movement of the cylinder. The *descender button* is a 3/2-es directional, mono stable valve, with spring returning.

For the safety function, the circuit contains an *Emergency STOP* button. This is a 3/2-es directional, bistabile valve, whit spring returning. If the Emergency STOP button is pushed, the valve is cuts the source air pressure from the circuit and the 5/3 valve stands into the center position.

The engineer can sets the air pressure with the *pressure controller valve*. This valve controller is a rotary button on the interface. The engineer can adjust the pressure between wide limits.

3. INTERFACE

Every valve, which is in contact with the operator, is going out to the interface. The other point in the safe working list, the emergency stop button is in the interface too. The pressure and speed controller dials are got a place on the interface. The manual of the machine must be on clearly visible place on the interface [1].

4. SIZING

4.1. Choosing of the cylinder

The cylinder is the actuator part of the machine, because this tool transforms the moving (in our case the cuter moving). In the choosing and sizing process the acting forces are the start points both of them the regulation of the food industry.

The sizing processes have been started with the cylinder type choosing. The FESTO has cylinders from stainless steel, which material is used in the food industry. The stroke length is depend on the size of the cheese which is known from the requirements list. The height of the cheese is 150 mm (C), we need some place for the positioning (P) is 100 mm and, for the full height cutting we need the thickness of the blades' frame (I) which is 25 mm. These distances are showed by the Figure 3.

$$S = C + P + I \quad (1)$$

The S stroke length is 275 mm, from the (1) equation. After then, the piston diameter has been determined. For the diameter, we have to know the cutting forces, which can calculate from the (2) equation:

$$F_C = F_{CCA} + F_{mc} + F_{mp} \quad (2)$$

Where:

F_{CCA} : The force for the blades cut the cheese totally [N]

F_{mc} : The mass of the cheese [N]

F_{mp} : The mass of the cutting platform [N]

We use the results from the cheese cutting experience, which made by another team member. He said the F_{Cc} force on one blade is 1700 N.

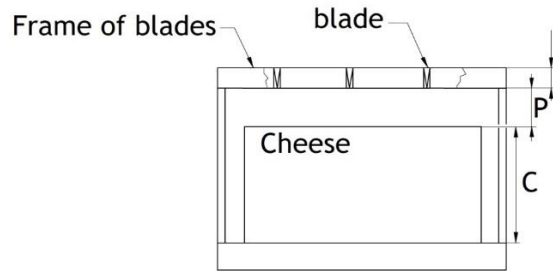


Figure 3. The cutting chamber with the cheese

For 3 blades (because the machine cut the cheese for 4 parts), as we do in (3) equation:

$$F_{CCA} = 3 \cdot F_{Cc} \quad (3)$$

From the (3) formula the F_{CCA} force is 5100 N on the three blades. The next force, which the piston has to explicate, the mass of the cheese, because the piston raises it. For the calculation we get the pack of the *Gouda* cheese. A general pack of the *Gouda* is a block with 300 mm diameter (r), 75 mm thickness (h) and 4 kg mass (m). From the (4) formula we get the volume V :

$$V = r^2 \cdot \pi \cdot h \quad (4)$$

We can count the density of the *Gouda* ρ from the (5).

$$\rho = \frac{m}{V} \quad (5)$$

From this point, we easily get the mass (m) of the block of cheese with the (6) formula, which we use in this project:

$$m = V \cdot \rho \quad (6)$$

Where:

V : the volume of the block [which is calculated from the (7) equation]:

$$V = a \cdot b \cdot c \quad (7)$$

Same way we can count the mass (m) of the *Kaskaval* cheese block, which is as type as the *Gouda*'s block, from the (6), and we know the density of the *Kaskaval* is 230 kg/m^3 .

We continue the task with the mass of the *Gouda*; we make this decision, because this cheese is harder, than the Kaskaval. The force F_{mc} , from the (8) formula.

$$F_{mc} = m \cdot g \quad (8)$$

The mass of the cutting platform is depending from the design and the material. From my team members, we know the mass is 14 kg. After then we multiply with the gravity coefficient (9) formula, and the F_{mp} is 137.34 N.

$$F_{mp} = 14 \cdot g \quad (9)$$

Where the g is the gravitation coefficient and, this is 9.81 m/s^2 .

From the (2) equation, we get the cutting force F_C ,

I calculated some plus force the safety, this plus is 10% of the F_C , and we need this, because we have not got cutting force dates from the Kaskaval cheese, consequently the F_C force is 5900N.

The results are included the *Table 1*.

Table 1.
The results of the calculations

Number of equation	Data	Result	Dimension
3	F_{CCA}	5100	N
4	V	$5.3014 \cdot 10^{-3}$	m^3
5	ρ	752.72	kg/m^3
6	m	6.9	kg
7	V	0.03	m^3
8	F_{mc}	221.5255	N
9	F_{mp}	137.34	N
10	F_C	5458.8655	N

We can open the catalog from FESTO's stainless steel cylinders, and I found the *Table 2*:

Table 2.
The main properties of the cylinders [2]

Force [N]							
Piston \varnothing	32	40	50	63	80	100	125
Theoretical force 6 bar, advancing	482	753	1178	1870	3015	4712	7360
Theoretical force 6 bar, retracting	415	633	990	1682	2720	4418	6880

As you can see on the *Table 1* the piston with 125 mm diameter will fulfill the requirements. The chosen cylinder is: RDNG 125 275 PPV. In this type code the RDNG means the type of the cylinder. The number of 125 is the diameter of the piston rod and the 275 is assigning the length of the rod. The PPV abridgment says

the type of the attenuation of the piston head, and this exactly pneumatic cushioning, self-adjusting at both ends. This cylinder type is showed by the *Figure 4*.



Figure 4. The chosen cylinder type [2]

After that I checked the piston rod for buckling. For the good working of the piston, this calculation is important. At first, I determined the end-condition of the piston rod, which is the fixed-fixed type; because both end of the rod are do not include joint-pins. We can understand this choosing from the *Figure 5*.

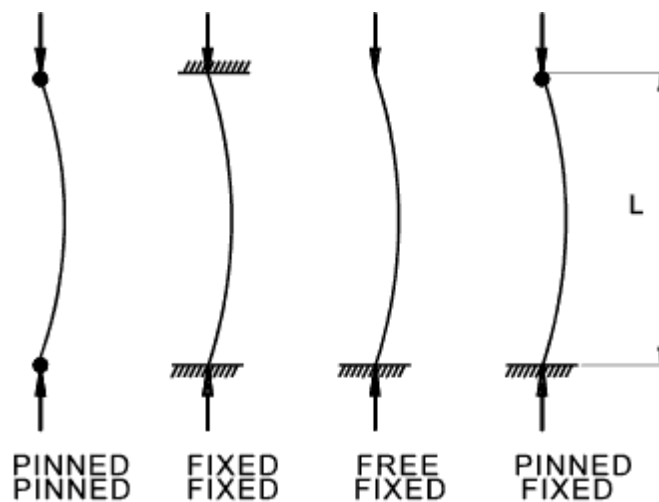


Figure 5. The buckling end-conditions [4]

This end-condition type releases the effective length (l_{eff}) from the (10) formula:

$$l_{eff} = 0.5 \cdot L \tag{10}$$

Our piston rod's length is 275 mm from the (1) equation, from that data the effective length is 137.5 mm. This data is required for the slenderness ratio calculation, which is showed by the (11) formula:

$$\lambda = \frac{l_{eff}}{k} \quad (11)$$

Where:

λ : Slenderness ratio

l_{eff} : Effective length [mm]

k : Radius of gyration [mm]

The radius of the gyration is calculated from the (12) equation:

$$k = \frac{d}{4} \quad (12)$$

Where:

d : diameter of the piston rod

In this case the d is 32 mm, so the k factor is 8 mm. If we have the l_{eff} and the k , we can get the slenderness ratio, which is in this task 17.188. In the next step I saw the graph, which show the critical values of the slenderness ratio, and the buckling method of that values, in the *Figure 6*.

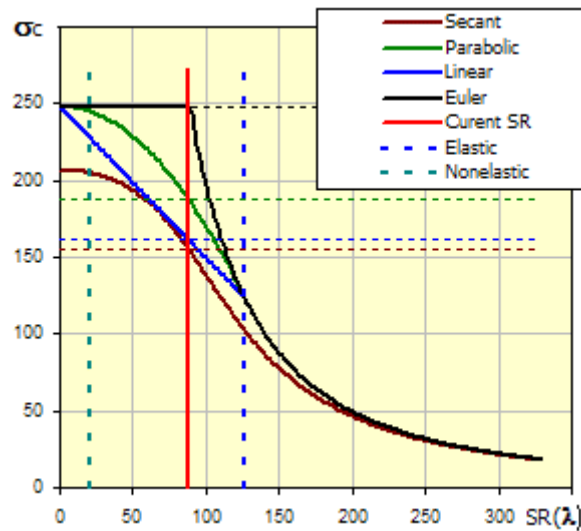


Figure 6. The context between the slenderness ratio and the buckling method [5]

Slenderness ratio in this task is 17.188, which is under the slenderness ratio of the red line in the *Figure 6*, it follows that, the rod is right, because the failure is not caused by the buckling in the working process, and we do not need more calculation [6].

4.2. Choosing of the valves

The main standpoint in the valve choosing progress is the flow. Besides that it was important is the operating. The 5/3 valve is pneumatic operated, the other valve is hand operated, with spring return. Pressure controller valve: LRMA-1/4-QS-6. In the

choosing of the valves is a main point the connection types, it is important if we want to connect the valves in one circuit.

- 3/2 directional valve: VHEM-PTC-M32C-M-G18
- 5/3 directional valve: VL-5/3G-1/8-B1
- Emergency STOP: KH/O-3-PK-3
- Speed controller valve: GPR-160-1/8-AL
- Air preparer unit: MSE6-E2M-5000-FB37-AGD

In the pneumatic lab of the University of Miskolc I can build the circuit for testing.

5. FINITE ELEMENTS MODELLING

Basic of my calculations, the piston rod get almost 5900 N presser force, and I was curious, this force how much deformation causes on the rod. I analyzed the rod, because in my opinion this part of the system gets the biggest load.

A simplified model of the rod has been made in Solid Edge software, and the analysis has been made in Ansys. With this program, we can simulate a lot of loads from the engineering practice. As we can see on the under figure, I create a mesh on the model of the rod in the *Figure 7* shows.

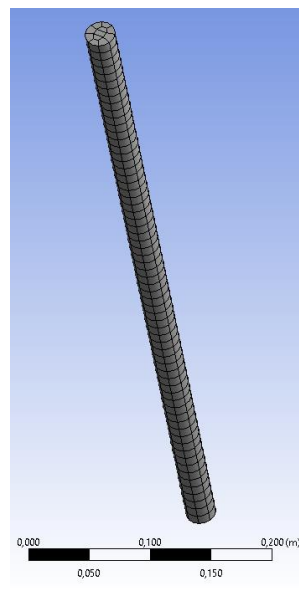


Figure 7. The rod after meshing

Secondary, the surfaces is marked, where the support is, and where the force's attack point is. After then, the force's value and direction are set, and the simulation is begun. The total deformation and equivalent stress are analyzed. Some surface in the rod is cut, because I want to see the stress' parameters inside the body of the rod.

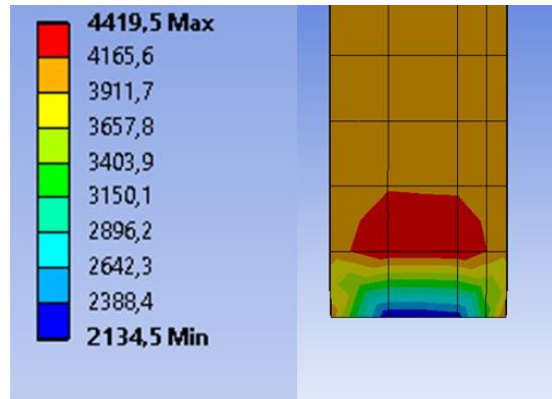


Figure 8. The stress in the rod, the support's side, and the scale in Pa

The left side of the Figure 8, the test bench has a scale, where the minimum and maximum values are readable of the stress and deformation. In my simulation the maximum stress is inside the rod and this value is: 4419.5 Pa. The maximum deformation is $1.3613 \cdot 10^{-8}$ m.

After then, I look for the Table 3, which contains the limit values of the stainless steel stress. The lowest non-proportional extension with 125 mm diameter is the 180 MPa, and the alloy is the X 3 CrNi 19 11 [7].

3. Table

The X 3 CrNi 19 11 stainless steel alloy parameters [8]

Mechanical properties at room temperature			
Size	R _{p0.2} [MPa]	R _{p0.1} [MPa]	R _m [MPa]
d ≤ 160 mm	180	215	460–680
160 < d ≤ 250 mm			
s ≤ 100 mm			

The diameter meets the requirements.

After that I made a test for buckling, that important because the high value of the buckling is disturbing the working of the piston. I stayed with the Ansys program, and I did the beginner steps like the previous analyzation. The support and the effective interface the same, just like the force, but now I am solving with the buckling. The test's result is showed by the Figure 9. The red color signs the biggest buckling in the time period of the force working. At the support surface the buckling is zero, and this area is signed with blue color. The simulation visualization is overacting for the easier understanding.

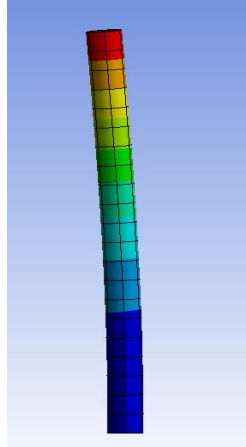


Figure 9. The buckling test's result

Important information from the test is the value of the load multiplier. In this case this value is almost 27.2, and this means, we can use the working force 27.2 times and the rod is buckling enough for the dysfunction. From above that value the rod buckling to lot for the normal working, and this test confirms the calculations in the chapter 5.

This test confirms to the statement, which says: the parameters of the rod meets the requirement.

6. POSSIBILITIES OF DEVELOPMENTS

If I want to connect this system to a production line, it has to contain some plus cylinders and movements, which triggers the in loads or out loads the cheese. With a cascade circuit we can do that. With two cylinders, the system is solving the cheese cutting and the cheese transportation. This process can be automated. However the two cylinders increase the costs of the system, and the machine, because the system needs more valves and more tubes. The cylinders flow chart is presented by the Figure 10.

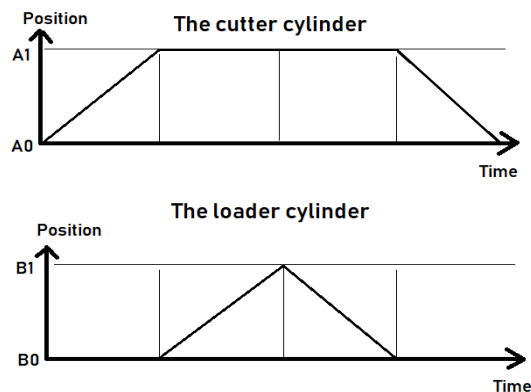


Figure 10. Flow chart

The loader cylinder can push the cheese on the cutter surface, or push out the pieces of the cut cheeses, above the blade to a conveyor belt.

7. CONCLUSIONS

In the *Figure 11* shows the 3D model of the machine, which we designed. We did not use of the roller conveyor, because the load process is solving manually. I think this construction meets all expectations.

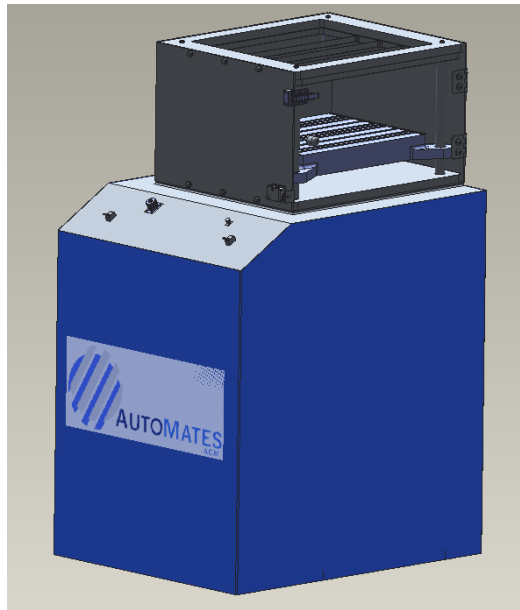


Figure 11. The Model of the cheese cutter machine

This project was very useful, one part, we can develop our professional language, and we were able to practice it, and the international teamwork. We met other culture thinking mode and problem solving. The weekly team meeting gives possibility to the discussion of the ideas and talk about the task and problems. And we can see I use the result of experiments, which was made by another team member, this need high reliability.

The topic of the project was good, because it was a real-life problem, with the engineer can meet easy in the career. I enjoyed it, because the upper points and it gives me some, if not so much, experience about the system designing, and team working.

I would like to thank for the professors, who help us while we solving the problem, and help for me to write this article. Without this help, we did not study so many useful things about the real life problem solving.

REFERENCES

- [1] Lajos Gáspár (1988). *Tejtermék-feldolgozás munkavédelmi követelményei*. Budapest: Népszava.
- [2] Depper, W. & Stoll, K. (1978). *Pneumatika gyakorlatban*. Budapest: Műszaki Kvk.
- [3] György Fábry (1995). *Élelmiszer ipari eljárások és berendezések*. Budapest: Mezőgazda.
- [4] <http://www.roymech.co.uk/images/struts.gif> (2018/10).
- [5] http://www.mitcalc.com/images/buckling_2_en.gif (2018/10).
- [6] Diószegi György (1984). *Gépszerkezetek méretezési zsebkönyve*. Budapest: Műszaki Könyvkiadó.
- [7] *Direct Line rozsdamenets acélok jellemzői katalógus* (2018/02).
- [8] Donald Peckner & Irving Melvin Bernstein (1977). *Handbook of stainless steels*. New York: McGraw-Hill.

FRICITION ASSESMENT OF LUBRICATED STEEL SURFACES I.

GÉZA NÉMETH

Institute of Machine and Product Design
3515 Miskolc-Egyetemváros
machng@uni-miskolc.hu

Abstract: The coefficient of kinetic friction is a random variable. Its value is governed by a huge number of circumstances. Studying some widely known methods, one of them was improved and made applicable to analyse the rolling resistance of antifriction bearings. The rolling resistance depends mainly on the load, the type of supplied lubricant, the number of speed and the service temperature. Although the suggested test rig is currently under development, it seems to be able to select the proper lubricant for the given installation environment and operation conditions.

Keywords: *sliding friction, rolling resistance*

1. INTRODUCTION

There are many ways to interpret the coefficient of friction. The Coulomb's law of friction might be said to be true, of course. According to this law the coefficient of friction depends on the quality of surfaces are in contact with and moves relatively to each other. This well-known attitude has been refined by many researchers and with many considerations during the last centuries. Only a few questions of them would be mentioned in our paper, noting that the tests were restricted to steel surfaces.

1. Is there any medium (fluid, solid <solid coating> or both) between the surfaces?
2. In what physical-chemical conditions are the surfaces?
3. What is the roughness of the surfaces and the value of the normal force acting between the surfaces? What friction state is made by the fluid, the coating and the relative sliding speed together?
4. What is the ambient pressure and temperature?
5. What additional processes (wear, temperature increase) occur and to what extent?

Taking these simple issues into account may be possible through the collaboration of several disciplines. Numerous professional books, e.g. [1], scientific theses, e.g. [2] were completed on the subject, using the opportunities for measuring and modeling at the technical standard of their era. The objectives of our paper are to demon-

strate some general and special experimental possibilities to clarify the friction conditions between machine parts and to contribute modestly to the extension of measurement experience.

2. DETERMINATION OF THE FRICTION COEFFICIENT

The measurement of the friction coefficient is based on any physical principle. The method may be general or may be specialized to a kinematic pair. *Figures 1* and *2* show well-known general principles for the determination of static and dynamic friction coefficient, respectively. These principles are based on angular and force measurement, respectively. *Figure 3* shows a principle for clarifying the dynamic friction between the kinematic pairs of a power screw [3]. It is used to determine the torque need for raising or lowering the load stress load, and according to the well-known calculating model, the dynamic friction coefficient of the screw-nut relationship. The force vector \vec{F} at the *Figure 3* includes the weight of the screw, rope drum and load. The torque generated due to the incrementally added m masses on the rope drum with diameter D , overcomes the friction torque of the screw and starts its rotation. In the case of a right-hand screw, the outlined figure corresponds to the case of raising the load. The torque equilibrium expressed by (1) is

$$Dmg = F \frac{d_2}{2} \operatorname{tg}(\rho' + \alpha), \quad (1)$$

of which the static coefficient of friction, μ_0 is countable, knowing the mean diameter, d_2 , the lead angle, α and the thread profile angle, β , i.e.

$$\mu_0 = \cos\left(\frac{\beta}{2}\right) \operatorname{tg}\left[\operatorname{arctg}\left(\frac{D}{d_2} \cdot \frac{2mg}{F}\right) - \alpha\right]. \quad (2)$$

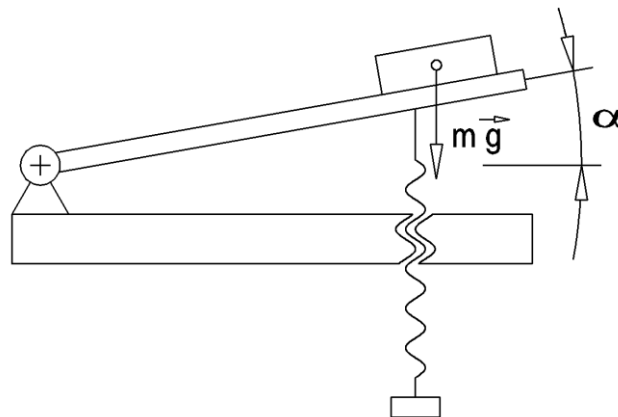


Figure 1. Measurement of static friction coefficient

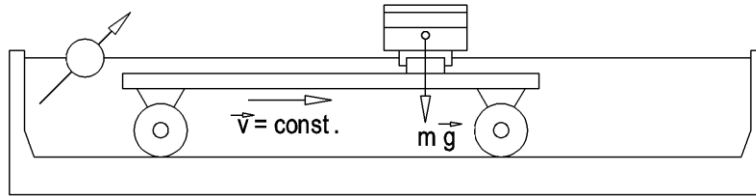


Figure 2. Measurement of dynamic friction coefficient

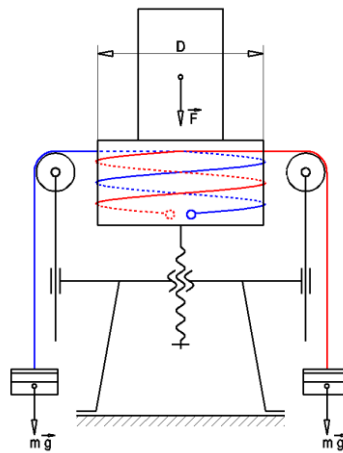


Figure 3. Measurement of friction torque between screw and nut [3]

There are other methods for measuring the coefficient of friction such as the principle of harmonic motion [3]. Let's rush through the known process. *Figure 4* shows two pulleys, rotating oppositely to each other, at a given distance, c apart from each other. The horizontal straight rod lying on the pulleys has a reciprocating motion. The force vectors designate that of acting to the rod.

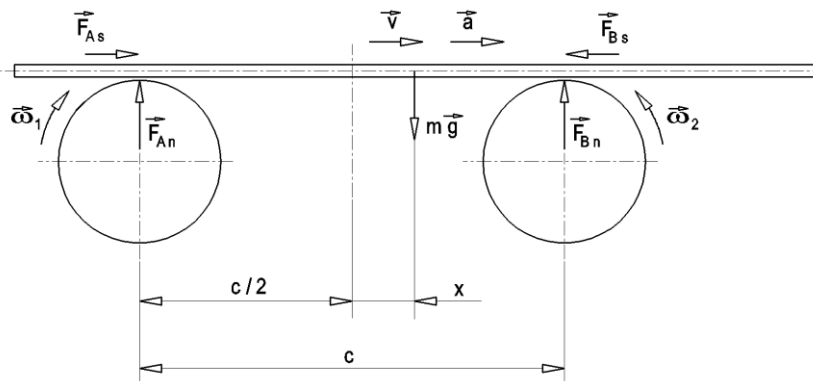


Figure 4. Kinematic and dynamic relations of the system [3]

3. THE USED PRINCIPLE OF THE MEASUREMENT

A homogeneous second order linear differential equation,

$$\ddot{x} + \frac{2\mu g}{c}x = 0. \quad (3)$$

applies for the problem of Figure 4., where the coefficient of dynamic friction, μ is unknown, the acceleration of gravity, g and the centre distance of the pulleys, c are known. The momentary displacement of the centre of gravity of the horizontal rod, x and its momentary acceleration, \ddot{x} are in the equation. Designating the multiplication factor of x by ω^2 , the general solution is

$$x(t) = \alpha \cos(\omega t) + \beta \sin(\omega t). \quad (4)$$

This $x(t)$ function is really the solution of the equation (3) where considering the initial conditions [at $t = 0$, $x(t) = \alpha$ and $\dot{x}(t) = 0$ cause $\beta = 0$], the solution of the simple harmonic motion is

$$x(t) = \alpha \cos(\omega t), \quad (5)$$

where α is the amplitude of vibration and that of the circular frequency is

$$\omega = \sqrt{\frac{2\mu g}{c}}. \quad (6)$$

Measuring the periodic time of the vibration, T , the coefficient of dynamic friction is

$$\mu = \left(\frac{2\pi}{T}\right)^2 \frac{c}{2g}. \quad (7)$$

4. TEST RIG IMPLEMENTATION

The practical implementation of the conceptual assumption presupposes the lateral guidance of the vibrating horizontal rod. A circular cross-section rod suitable to move on the disks (pulleys) made of the inner ring of a deep groove ball bearing. The curvature relations are similar to that of the ball bearing, shown in *Figure 5*. On the inner ring of the bearing 6312, the main curve radii of the ball race are 36.4 mm and 11.5 mm, the balls have a diameter of 22.2 mm. Accordingly to this geometry, a rod with diameter of up to 22 mm is suitable for the 72.8 mm diameter discs. It is advisable to increase the centre distance of the disks to make the rod more balanced. Based on the description of the principle of measurement and the result of formula (7), it follows that under Earth conditions, in the case of fixed rotary axes, the result

of the measurement depends only on the centre distance, c . It is independent of the speed of the discs, so they can be different. The truth of this state is probable at dry friction, low speed and under normal atmospheric and temperature conditions. However, due to the simplicity and the later extension of the measurement conditions, the speed of rotating discs are chosen to be the same.

Lining up four gears of the same number of teeth, the opposite direction of rotation and the same speed of the pulleys can be assured [3]. Revolving the pulleys in the proper direction the rod is moved inwards.

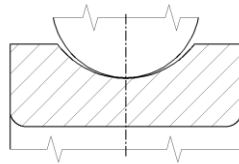


Figure 5. Curvature relations in a deep groove ball bearing



Figure 6. Powertrain of the pulleys

In the drive arrangement shown in *Figure 6*, the third gear (counted from left) is rotated clockwise to produce the desired motion conditions. The amplitude of reciprocating motion can be set to $0 < \alpha < c/2$ according to the initial condition. The amplitude cannot have a value close to the limits of the range, partly to make it easier to detect vibration movement and partly to balance the rod.

In case of dry friction, the friction coefficient is expected in the range of $10^{-1} < \mu < 10^1$, depending on the ambient temperature and pressure [1]. Let the periodic time of motion be in the range of $2,5s > T > 0,25s$. This periodic time allows the accurate detection of vibration, even visually. Due to equation (7), this corresponds to a $c = 10,3106 m$ centre distance. *Figure 6* shows uncorrected (without any profile correction) spur gears. The number of teeth, $z = 34$ and the module, $m = 3 mm$. The centre distance, c of the two pulleys is $c = 3a = 3zm = 306 mm$, which fulfils the former criterion.

5. POSSIBLE TEST CIRCUMSTANCES

The measuring device is able to determine the sliding friction coefficient, originally in the case of dry friction. The drive is also insensitive to the speed and the rolling resistance of the bearings. Due to the practical value of the friction coefficient, the relatively large periodic time makes the air resistance to be negligible. Any circumstance that reduces friction coefficient, e.g. lubrication, increases the periodic time, T which improves the accuracy of the given test method.

In the case of dry friction, the presence of low temperature and vacuum influence more strongly the value of the sliding friction coefficient. The effects of sliding speed and the curvatures are not significant. For lubricated surfaces, however, all other factors that may affect the lubricating condition should be considered. The most important factors are:

- The phase of lubricant
 - Gas,
 - Liquid,
 - Consistent (greases),
 - Solid (dry).
- Other properties of the lubricant
 - Viscosity,
 - Consistency,
 - Time-dependent rheological properties.
- Mixing additives to the lubricants,
- Roughness and pattern of the ball race of disc and the rod surface,
- The curvature of the disc and rod,
- The rotational speed of the disks,
- The loads on the surfaces,
- Possible solid surface coatings.

The above factors have a very high impact to each other, so the test possibilities are very wide. Without the necessity of completeness, some interesting cases should be mentioned.

- The rod is very light, made of steel tube with very small wall thickness and the disk has a very high peripheral speed. An aerodynamic lubrication condition may occur between the contacting surfaces. The coefficient of friction may fall below $\mu = 10^{-1}$, which results a significant increase in the periodic time of the harmonic motion.
- In case of fluid friction, the peripheral speed is also important because the friction condition is influenced by the viscosity of the lubricant, the highest asperities of the rough surfaces and the loading of the surfaces.
- In the case of grease lubrication, at very low temperature, both the viscosity of the base oil, forming grease, and the consistency of grease are decreasing. There is a need for time to distribute the lubricant to the correct lubricity.

While the lubrication condition is defective, no safe separation of metal surface asperities is achieved.

- The friction-reducing effect of some soft-metal coatings is only applied in case of higher loads [4], therefore, it is necessary to create a gradual increase in load. The simplest way is the loading of the rod having properly stiff at its ends so that the symmetry of the loads remains. The increment of air resistance cannot be considerable if the conditions of simple harmonic motion should be provided later on.

The test rig was made from the elements shown at *Figure 6*. The shaft of the third gear is driven by a controllable speed step motor through timing belt drive. *Figure 7* shows a measurement compilation. The room temperature was 22 °C. The electric motor is driven through a power supply. The adjusted speed is about 500 rpm, the rod and the disks are lubricated slightly by rolling bearing grease, made of mineral oil, viscosity $\nu_{40\text{ °C}} = 97 \text{ mms}^{-1}$ with barium complex soap thickener, NLGI grade is 2. The solid rod diameter, $d = 15 \text{ mm}$, its length, $l = 1.1 \text{ m}$. The measured periodic time was $T = 2.4 \text{ s}$.

A similar measurement was made in dry condition. The rod was a hollow cylinder of outer diameter, $d = 16 \text{ mm}$, wall thickness, $s = 1 \text{ mm}$ and length, $l = 0.5 \text{ m}$. The other circumstances were as the previous one. The periodic time was $T = 2.0 \text{ s}$. The counted coefficients of dynamic friction, due to formula (7) are 0.107 and 0.154, respectively.

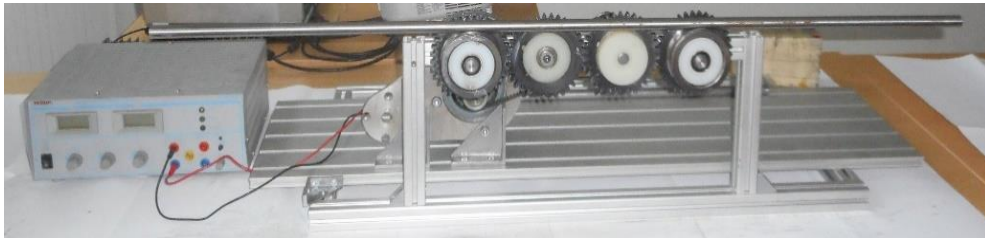


Figure 7. The test rig. Rod and disks are lubricated slightly by grease

6. EXTENSION OF THE TEST PRINCIPLE

The principle shown in *Figure 4* and the experimental apparatus shown in *Figure 7* assume that the four gears with the same number of teeth determine unambiguously the speed of the discs on the first and last axes, and the average sliding speed between the disks and the reciprocating rod will be permanent. Let's modify this principle to make the test rig suitable for measuring rolling resistance of rolling bearings and for studying the effect of lubricant and ambient temperature on rolling resistance. *Figure 8* shows the modified principle.

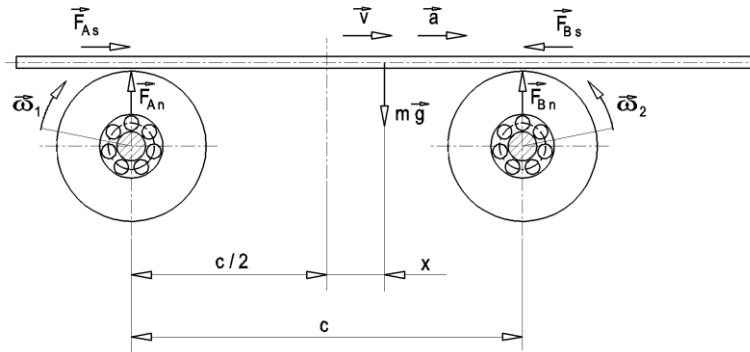


Figure 8. Modified principle. The disks are revolved only by the rolling resistance

In contrast to the original task, only the inner ring of the bearings that support the disks are rotated. The outer rings and the discs rotate only due to rolling resistance. The rolling resistance is influenced by the part of mass of the rod, the mass of outer ring of bearing and the mass of the disks. The friction force between the disks and the rod is considerably larger than the rolling resistance of the bearings, and the friction force acts at much greater arm than the rolling resistance, so the rod will not slip on the discs. If the rod accelerates, the angular acceleration of the disks can be linked unambiguously. It can also be clarified that the angular accelerations of the two disks are equal in magnitude and direction, due to the clear rolling between the disks and the rod. Not only the rod, but the disks perform harmonic motion, and it is expected that the vibration will be unattenuated as well. To formulate the motion equation for the left-hand disk, Figure 9 illustrates the diameters d and D , the mass moment of inertia, J , the outer forces, F_s and F_g , and the angular acceleration, ε .

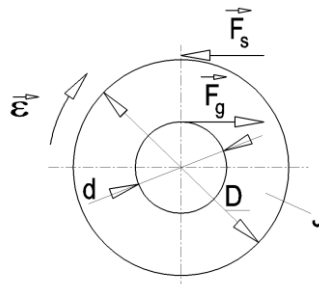


Figure 9. Data for the equilibrium of the left hand disk

The normal force acting to the disk from the rod, due to Figure 8 is

$$F_n = \left(\frac{1}{2} - \frac{x}{c} \right) mg. \quad (8)$$

The normal force acting upwards from the balls to the outer ring of the bearing is completed by the sum of the disk and the outer ring of bearing, $m_t g$. The equation of the torques from the external forces and the acceleration moment in the case of the left disc, with the symbols of *Figure 9* is

$$\frac{d}{2}F_g - \frac{D}{2}F_s = J\varepsilon. \quad (9)$$

from which the friction force F_s can be expressed and its value is much smaller than that of the problem of *Figure 4*. The rolling resistance from the supplemented equation (8) is

$$F_g = \mu_g \left[\left(\frac{1}{2} - \frac{x}{c} \right) mg + m_t g \right]. \quad (10)$$

To obtain the friction force acting at the circumference of the left side disc, the instantaneous acceleration of the rod, $\ddot{x} = \varepsilon D/2$ should be considered, and equation (10) should be substituted into equation (8), i.e.

$$F_s = \frac{d}{D} \mu_g g \left[\left(\frac{1}{2} - \frac{x}{c} \right) m + m_t \right] - \frac{2}{D} J \varepsilon. \quad (11)$$

The formula of the friction force acting at the circumference of the right side disc is similar. The angular acceleration of this disc is the same, both in magnitude and direction as that of the left side disc, i.e.

$$F_s = \frac{d}{D} \mu_g g \left[\left(\frac{1}{2} + \frac{x}{c} \right) m + m_t \right] + \frac{2}{D} J \varepsilon. \quad (12)$$

The motion equation of the horizontal rod, obtained from Newton's second law, similarly to equation (4) is a homogeneous second order linear differential equation, i.e.

$$\ddot{x} + \frac{\frac{d}{D} \frac{2\mu_g g}{c}}{1 + \frac{8J}{D^2 m}} x = 0. \quad (13)$$

Comparing this to the simpler equation (4), there are some extra influencing factor, as the mass of the rod, m , the diameter of the ball race at the outer ring of the investigated bearing, d or the diameter, D and the mass moment of inertia, J , of the discs, as *Figure 9* shows. J also involves that of the outer ring of the analysed deep groove ball bearing and the hollow disc between the bearing and the pulley of the horizontal rod.

Here the periodic time, T of the simple harmonic motion is measurable, so the circular frequency of the vibration is countable, i.e. $\omega = 2\pi/T$. At last, the coefficient of rolling resistance of the investigate bearing is

$$\mu_g = \frac{D}{d} \left(1 + \frac{8J}{D^2 m} \right) \omega^2 \frac{c}{2g}. \quad (14)$$

The only uncertainty in the calculations is caused by the determination of the mass moment of inertia, J of the elements between the balls of the analysed bearings and the horizontal rod.

7. PRACTICAL APPLICATION OF THE USED TEST PRINCIPLE

The elements shown in *Figure 6* or the test rig at *Figure 7*, following the theoretical solution of *Figure 4*, is suitable to test the sliding friction between cylindrical and toroidal surfaces which has point contact and both the speed and load may be varied. The Hertzian stress calculated at the maximum adjustable load (to be described later) in the contact between the inner ring of a deep groove ball bearing 6312 of *Figure 5* and a 22 mm diameter cylindrical bar is approximately 320 MPa, well below the allowable practical values. The measurement of dynamic friction coefficient is possible with or without lubrication. The favoured lubricant is grease. Supplying and removing the lubricant on or from the surfaces, respectively can be carried out quickly and easily. The free choice of lubricant type is limited by load and temperature range. Any type of oil lubrication would require a closed gearbox.

The toroid surface of the disks (ball race of the bearing) is made of quenched chromium steel. The material quality and roughness of the rod surface can range from cold drawn normalized unalloyed tool steel to grinded, hardened high alloy steel. Increasing the load is possible with symmetrically located masses at the ends of the horizontal rod. The magnitude of the masses is limited by the usual degree of allowable deflection of the axles. Let this value be $y_{all} = 0.3 \text{ mm}$ in the case of a cylindrical steel bar with a diameter of 22 mm and a length of 0.9 m, for which considering the centre distance, c the overhanging ends can be loaded up to a maximum of 3 kg mass, in addition to the own mass of the rod of almost 3 kg.

Reduction of the load can be achieved by choosing a cold-drawn precision steel tube of 1 mm wall thickness, in this case its own weight is below 0.5 kg, so it is possible to test lubricating greases with less consistency and lubricating oils of lower viscosity.

The ambient temperature of the test does not deteriorate the accuracy of the measurement within a permissible limits, so it is possible to detect degradation of the lubricant caused by the lower temperature ranges.

According to the principle shown in *Figure 8*, the rolling resistance of rolling bearings can be tested. The practical implementation of the measurement requires further considerations since it is necessary to solve both the easy and quick insertion of the bearing and the changing of tested lubricant in the measuring rig.

8. FURTHER TASKS OF THE MEASURING RIG

The rotation of the disks is carried out by a variable speed electric motor. In case of the need for high sliding speed changes, the replacement of the electric motor and the gear unit can be solved, too. The number of revolutions of the discs can be measured using a mechanical counter or an inductive encoder and a recapitulative device.

The total number of vibrations carried by the rod can also be measured by an inductive transducer, receiver and summing counter. The magnetic encoder may be attached to the centre of the rod and the receiver head is fixed to the stand. The summing counter also measures the time t of the test. The summing counter connected with the receiver counts the passes, N at the equilibrium position. The periodic time, T is twice the ratio of the usual one, i.e. $T = 2t/N$.

9. SUMMARY

By studying a well-known sliding friction measurement principle, the authors have been able to clarify the basic principles of the operation of a device applicable to test the rolling resistance of a given deep groove ball bearing supplied by any type of lubricating grease, at an adjustable operating temperature, thereby detecting a special ability of a particular grease.

ACKNOWLEDGEMENT

This work was supported by the European Union and the Hungarian State, co-financed by the European Regional Development Fund in the framework of the GINOP-2.3.4-15-2016-00004 project, aimed to promote the cooperation between the higher education and the industry.

REFERENCES

- [1] Bowden, F. P. & Tabor, D. (1950). *The Friction and Lubrication of Solids*. Part I. publ. Oxford: Oxford University Press.
- [2] Balogh T. (2007). *Érintkező felületek száraz súrlódásakor lejátszódó folyamatok numerikus és kísérleti vizsgálata*. PhD-értekezés. Budapest: Budapesti Műszaki és Gazdaságtudományi Egyetem.
- [3] Oulsnam, S. R. & B. G. Brothers (1960). *Engineering Laboratory Work. Part 1. Applied Mechanics S.3*. London: Cleaver-Hume Press Limited, pp. 38–44.
- [4] Valasek I. & Auer J. (2003). *Kenőanyagok és vizsgálataik*. Budapest: Tribotechnik Kft., pp. 54–55.

MICRO SWITCH FAILURE ANALYSIS

VIVIEN SIPKÁS–GABRIELLA BOGNÁR

University of Miskolc, Institute of Machine and Product Design
3515, Miskolc-Egyetemváros
machsv@uni-miskolc.hu

Abstract: The aim of this paper is to introduce the reliability methods in connection with lifetime, the moisture resistance test. Moreover, the way to the design of testing equipment using the method of design of experiment (DoE).

Keywords: *Accelerated Life Testing, Lifetime, Failure; Failure prediction; Reliability Prediction; Micro-switches; Acceleration Models*

1. INTRODUCTION

We shall understand the reliability that a product maintains its initial quality and performance at a certain period of time, cycle, distance etc. under given conditions without failure. These conditions include both environmental condition and operating condition. Environmental condition means a common natural ambience such as humidity, vibration, temperature and working condition means an artificial environment such as voltage, current load, place for installment and hours of use, which occurs during the life of the product [1].

It has already been stated in the previous article that the micro switches used in gardening machines unfortunately have several malfunctions [7]. Among others, due to the high temperatures, the deformation of internal components, the loss of function, switching and breaking of button switches can appear. In addition, the structure can be burned, and the contacting surfaces can be charred. For all these reasons, the switch will not work properly [7, 13].

The aim our investigations is to carry out pre-planned measurements and testing micro switches applied in garden tools. Therefore, we need an effective method for designing and analyzing experiments which allows objective conclusions to predict the lifetime of the examined switches.

2. ACCELERATED TESTS

Today's manufacturers face strong pressure to develop new products with higher technological content in record time while improving productivity, product field reliability and overall quality. This has motivated the development of such methods like concurrent engineering and has encouraged us to design experiments for product and process improvement. The requirements for higher reliability have increased the

need of testing the materials, the components and the systems. To achieve high reliability, it is necessary to improve the design and manufacturing processes.

In the literature we can find three different methods of accelerated reliability tests [11]:

2.1. Increase the use-rate of the product

Useful reliability information could be obtained in a matter of days instead of months.

2.2. Increase the aging-rate of the product

Increasing the level of experimental variables like temperature or humidity we can accelerate the chemical processes of certain failure mechanisms.

2.3. Increase the level of stress

In this last type we increase the level of stress, the temperature, the voltage, or the pressure during the tests comparing with the levels that units operate. A unit will fail when its strength drops below applied stress. Thus, a unit at a high stress will generally fail more rapidly than it would have failed at low stress.

Combination of these methods of acceleration are also employed. Variable like voltage and temperature cycling can both rate of an electrochemical reaction and increase stress relative to strength. In such situations, when the effect of an accelerating variable is complicated, there may not be enough, physical model for acceleration [11].

Combination of these methods are used in further stages of the research, because the micro switches will also be subjected to complex stresses.

3. ON THE PREDICTION METHODS OF RELIABILITY AND LIFE SPAN

The reliability prediction is to predict failure rate and average life span associated with reliability by taking operation, working environment and conditions associated with systems and parts into account. (*Figures 2–3*) refer to some types and measures of life span prediction. By conducting reliability prediction, manufacturers can predict product life span. Then, consumers can have a choice for product with longer life span. For components in the industry there are several prediction standards which allow us to predict failure rates of parts under a given system operation and working condition [3–6].

The *Figure 1* shows the lifetime prediction process that is primarily necessary to determine all the problems about the micro switches and their mechanism and physics of failure (see chapter 3.1. below). Simultaneously, it is necessary to test the lifetime of the micro switches. On the base of the flowchart, we are going to determine the acceleration models, – factors and then lifetime prediction.

The prediction will eventually be used mainly in design and product development stage of parts and system. Also, the prediction enables the operators to secure customer safety by building preventive maintenance plan in advance.

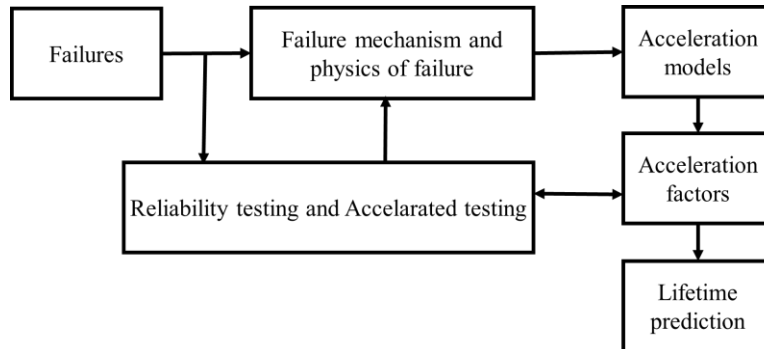


Figure 1. Lifetime prediction diagram [5]

Predicting the life span of parts and applying it to maintenance or conducting activities to promote longer life span by reflecting operation data feedback to a design are not yet a common practice and it is quite challenging.

Some examples are shown on the following figures (Figures 2–3), these include the type of life span prediction and its method given is by manufacturers.

3.1. Life Span Prediction by using field data

We introduce some examples on life span prediction and its method on Figure 2, which represents it secured field data with quality that meets statistically needed information. This is a good example of the previously collected failures.

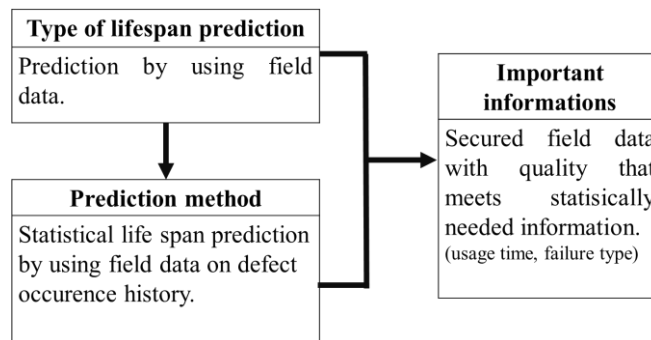


Figure 2. Lifetime prediction by operator as a prediction measure [1, 2]

Micro switches in garden tools may contain variety of faults, and our earlier publication has shown the most common types and the possible causes of their reasons [7, 13].

Typical failure problem is the wear of the micro switch’s switch-button, which could be the result of poor construction design, high switching numbers etc.

Furthermore, deformation due to high temperature. There are several reasons for this problem, e.g., overheats due to overload and higher number of switching.

Burning of contacting surfaces is also very common breakdown, the cause of problems is higher humidity, – vibration of machine and etc. The result is there will be extensive burned signs on the contacting surfaces due to temperature increasing, surfaces will being sooted.

When the circuit is closed and interrupted, an arc is created. The material migration is the consequence of this phenomena, due to the heat generation and the increase of the temporary resistance. It results the overheating of the pre-assembled components such as springs [7]. These failure modes should be taking into account according to the method of *Figure 2*.

3.2. Life Span Prediction by conducting an accelerated life test

This lifetime evaluation can be adopted by manufactures to be considered at development stage [2].

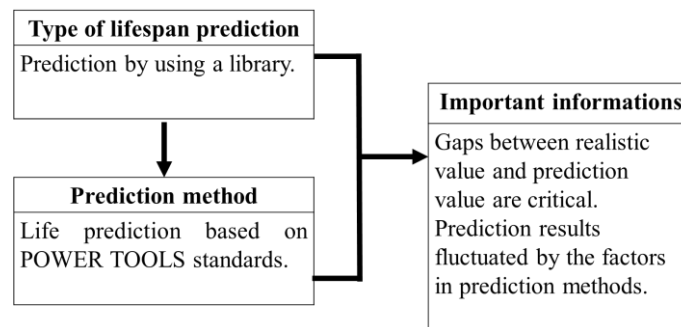


Figure 3. Life Span Prediction on the base of standards [1, 2]

Investigations can keep track of the research processes, which are often carried out according to appropriate standards. This is the IEC 60745-1 standard for handheld safety. Among the many chapters of the above standard, we apply the moisture resistance test, the essence of which is to place a given tool in the chamber and examine the temperature and humidity specified. Changing the temperature and humidity the micros witches operating the machines can have an operating effect. This test method is prescribed by the standard in an unladen condition. However, we would like to do it in a future laden state (e.g., switch operation) and not just a temperature and humidity range that is standard, but we want to do this by increasing both modes of use. As a first step, a standardized instruction is required and a test of an unladen condition has to be performed.

The humidity treatment carried out in a humidity cabinet containing air with a relative humidity of (90–100%) and room temperature is required. Before inserting into the air humidity chamber, the tool must be brought to a specified temperature, which is approximately a few degrees Celsius to approximately the operating state of a machine. Then we will be in the cabinet within the prescribed time limit for a specified period.

In order to achieve the specified conditions within the cabinet, it is necessary to ensure constant circulation of the air within and, in general, to use a cabinet which is thermally insulated [8].

4. DESIGN OF EXPERIMENTS

The term experiment is defined as the systematic procedure carried out under controlled conditions in order to discover an unknown effect, to test or establish a hypothesis, or to illustrate a known effect. When analyzing a process, experiments are often used to evaluate which process inputs have a significant impact on the process output, and what the target level of those inputs should be to achieve a desired result. Design of Experiments can be designed in many different ways to collect this information is an effective method for designing and analyzing experiments so that the data obtained allows for the deduction of real and objective conclusions. This method is a detailed experiment plan with settings and order that must be available before the experiment is completed.

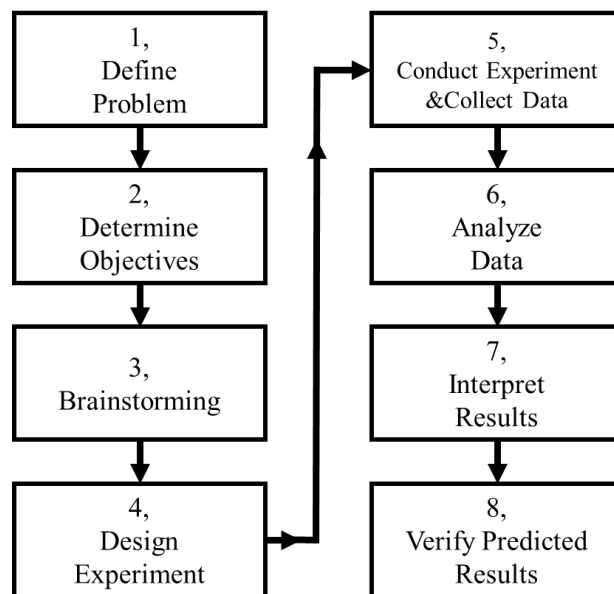


Figure 4. Design of Experiments Process [9]

Using the Design of Experiment method, we have already defined the problem that the micro switches used in gardening machines are far below the manufacturer's required edge. There are more failures than the waited.

Thus, we have to define the goal of constructing an equipment that can provide complex data set for more products. After the first two points have been defined, the process of thinking about the features of the device is taking place (Figure 4).

Designed experiments give the possibility of advanced and powerful analysis. An effective experimentation method can filter disturbing factors and discover significant process factors. The factors then can be used to control further testing. Well-designed experiments not only save time but also solve critical issues that are not yet visible in processes. Specifically, the interaction of factors can be observed and evaluated. Ultimately, we can find out which factors, results are counted, and whose life-span influences [9, 10].

5. CONCLUSION

In this paper the most important type of accelerated test methods, the prediction method of reliability and life span are considered. Two of these methods were introduced based on literature, which can be used in closely in the investigation of micro switches. By reviewing standards, we summarized that the most important steps of the moisture resistance test, which will be carried out in the further stages of the research, first according to the standards, and then with certain modifications at different higher temperature ranges, thereby increasing the load. After that, we considered the Design of Experiment method, which is an effective method for designing and analyzing and evaluating experiments.

ACKNOWLEDGMENTS



Supported BY the ÚNKP-18-3-I-ME/19. New National Excellence Program of the Ministry of Human Capacities”

REFERENCES

- [1] Jung-Geon Ji, Kun-Young Shin, Duk-Gyu Lee, Moon-Shuk Song & Hi Sung Lee (2012). Life Analysis and Reliability Prediction of Micro-Switches based on Life Prediction Method. *International Journal of Railway*, Vol 5, No. 1, March 2012, 1–9.
- [2] Shin, K. Y., Ji, J. G, Han, J. H, Lee, D. G, Son, Y. J. & Lee, H. S. (2011). *Life analysis and reliability prediction of relays based on life prediction method*. Spring Conference of Korean Society for Railway.
- [3] Reliability in electronic. Technical article. *The expert in power*, 1–11. www.xppower.com, 2018. 10. 15.
- [4] P. Bardos (1979). *Reliability in Electronics Production*. Proceeding of PCIM, Munich.
- [5] A. L. Hartzell et al. (2011). *MEMS Reliability, MEMS Reference Shelf, Lifetime Prediction*. DOI 10.1007/978-1-4419-6018-4_2, Springer Science + Business Media, LLC 2011, pp. 9–42.

-
- [6] European Power Supply Manufacturers Association (2005). *Guidelines to Understanding Reliability Prediction*. Edition 24 June 2005. www.epsma.org
- [7] Vivien Sipkás & Gabriella Bognár (2018). The Application of Accelerated Life Testing Method for Micro Switches. *International Journal of Instrumentation and Measurement*, pp. 1–5.
- [8] *General requirement for garden tools*. IEC 60745-1 Ed 4 2006-04
- [9] <https://www.moresteam.com/toolbox/design-of-experiments.cfm>, Date of download: 17. 10. 2018.
- [10] Márkus László (2018). Az ipari kísérlettervezés statisztikai módszerei. Educational supplement, date of download: 17. 10. 2018.
- [11] William Q. Meeker & Luis A. Escobar (1998). *Statistical Methods for Reliability Data*, Wiley-Interscience Publication–John Wiley & Sons.
- [12] Sipkás Vivien & Vadászné Bognár Gabriella (2017). Mikrokapcsolók gyorsított élettartam vizsgálata. *GÉP*, Gépipari Tudományos Egyesület Műszaki Folyóirata, 2017/4. LVXXIII. évfolyam, pp. 57–60. (in Hungarian)
- [13] Sipkás Vivien & Vadászné Bognár Gabriella (2017). Mikrokapcsolók élettartamának vizsgálata. *Jelenkori társadalmi és gazdasági folyamatok*, 12, pp. 95–102. (in Hungarian)

IMPLEMENTATION OF A SHELL LIKE THERMO ELASTO-HYDRODYNAMIC CONTACT ELEMENT TO A COMMERCIAL FEM SOFTWARE

SZABOLCS SZÁVAI¹–SÁNDOR KOVÁCS

University of Miskolc, Institute of Machine and Product Design
3515 Miskolc-Egyetemváros
szavai.szabolcs@uni-miskolc.hu

Abstract: Although several methods have been already developed for solving thermo elasto-hydrodynamic (TEHD) problems, the solution of the highly nonlinear problem is still quite challenging. So the development of a P-version FEM model for calculating the film shape, the pressure and temperature distribution and its implementation to commercial software seems to be timely to study the sliding-rolling materials during operation. Since the general 3D flow problem can be reduced to a quasi 2D case based on the hydrodynamic lubrication theory developed by Reynolds, special lubricant film element can be developed for finite-element modelling of such problems.

Keywords: *Elasto-hydrodynamic lubrication, Finite Element Method, Lubricant film element*

1. INTRODUCTION

The generalized case of surface pairs contacting along a spot in the status of liquid friction is illustrated in Figure 1. In the solution of a differential equation by variation method, the equation is put into an equivalent weighted-integral form and then the approximate solution over the domain is assumed to be linear combination ($\sum_j c_j \phi_j$) of appropriately chosen approximation function ϕ_j and undetermined coefficient, c_j . The coefficient c_j are determined such that the integral statement equivalent to the original differential equation is satisfied. Weak solution of the weighted integral forms of the governing Reynold and energy equations has been presented by Szávai [3] for TEHD problems. In this paper is enough to assume that the weighted-integral forms of the Reynold and energy equations look like:

$$\int_{A_c} w_R \cdot R_{Reynolds} \cdot dA = 0 \quad (1)$$

$$\int_{A_c} \int_{h_1}^{h_2} w_Q \cdot R_{energy} dz \cdot dA = 0 \quad (2)$$

The film shape can be calculated as a superposition of the initial geometry, the displacement of a rigid surface and the deformation of a half-space under pressure. After deformation, the film shape:

$$h = h_{g2} + \Delta_{rigid1} + \Delta_{rigid2} + \delta_1 + \delta_2 = h_g + \Delta_{rigid} + \delta \quad (3)$$

where h_g is the initial gap size, Δ_{rigid} is the relative rigid normal displacement between the contact bodies, δ is the total deformation of the surfaces.

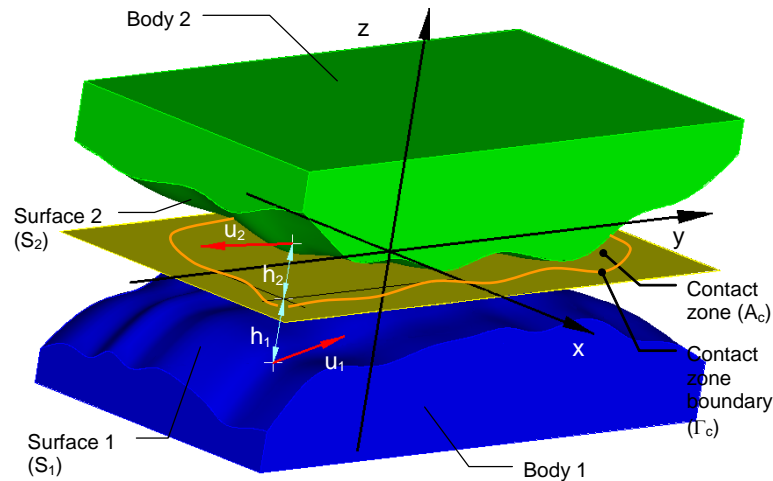


Figure 1. Contacting bodies

The calculation of displacements occurring under the effect of the distributed load acting on the surface is already a routine task in the range of numerical methods by now thus the equations needed for this will not be detailed either. The classical approach is to find the stresses and displacement in an elastic half-space due to surface traction [2]. Let us assume for the solution of this problem that the equation below is in existence:

$$L_{p_i} (p(x, y), \delta_{p_i}(x, y)) = 0 \quad (4)$$

For calculating the temperature of the contact surfaces range of numerical methods are available or the solution for moving heat source on semi-infinite half space [1] can be used as the substructure model when the analytical expression can be joined to the FEM solution by least squares approximation.

The integral of the pressure over the contact area should be equal with the external load.

$$F_W = \int_{A_c} p \cdot dA \quad (5)$$

F_W is the normal load of the surfaces. It can be satisfied if the Δ_{rigid} is a variable.

2. DIMENSIONLESS GAP COORDINATE AND DIMENSION REDUCTION

The equations (1) and (2) consists several integration through the thickness like $\int_{h_1}^{h_2} f(z)dz$ and $\int_{h_1}^z f(\bar{z})d\bar{z}$ in case of non-Newtonian lubricants or TEHD case. These integrals make the problems to be full 3D case. In order to reduce it to a quasi 2D case the integral domain has to be unified by transformation of the z coordinate.

As usual, it can be assumed that $h_1 = 0$ and $h_2 = h$. In this case let us introduce the dimensionless coordinate ζ along the gap as defined below and let the coordinate z is the linear function of ζ :

$$z = h \left(\frac{1 + \zeta}{2} \right); \quad \frac{\partial z}{\partial \zeta} = \frac{h}{2} \quad (6)$$

And consequently the integrals through the lubricant film thickness are:

$$\int_0^h f(z)dz = \frac{h}{2} \int_{-1}^1 f(\zeta)d\zeta; \quad \int_0^z f(\bar{z})d\bar{z} = \frac{h}{2} \int_{-1}^{\zeta} f(\bar{\zeta})d\bar{\zeta} \quad (7)$$

So the weighted-integral forms of the energy equation looks like:

$$\int_{A_c} \frac{h}{2} \int_{-1}^1 w_Q \cdot R_{energy} \cdot d\zeta \cdot dA = 0 \quad (8)$$

In this way the integration for the energy equation has to be carry out on a uniformed thickness domain and it makes possible to handle the problem as a quasi thick shell problem where the thickness of the shell is variable.

3. INTEGRATION TROUGH THE THICKNESS BY GAUSS QUADRATURE

In FEM based solutions the integrations are carried out in most cases numerically by means of Gaussian quadrature [4]. If the integral domain is defined through the full thickness $(-1..1)$, the integration above the dimensionless thickness is:

$$\int_{-1}^1 f(\zeta)d\zeta \approx \sum_{i=1}^n w_{G_i} f(\zeta_{G_i}) \quad (9)$$

Where ζ_G are n specified ‘‘Gauss’’ points within the domain of integration and w_G are weights at specified points [4]. The more applied Gauss point, the higher integration accuracy reached but the more computation time needed as well.

Determination of \bar{u}_{xy} and some of the viscosity functions for generalized Reynold equation requires integration above a semi undefined region $(-1..1)$ that has to be managed as well. Since the function $f(\bar{\zeta})$ can be determined at any point above the gap, let us take the Lagrange interpolation of the integrand above the $\bar{\zeta}(-1..1)$ region through $n + 2$ $(f(\bar{\zeta}_s), \bar{\zeta}_s)$ points where $\bar{\zeta}_s = (-1, \zeta_G, 1)$ and n is the number of the predefined ζ_G Gauss points:

$$f_{Lagr}(\bar{\zeta}) = \sum_{k=1}^{n+2} f(\bar{\zeta}_{S_k}) P_k^{n+1}(\bar{\zeta}) \quad (10)$$

where

$$P_k^{n+1}(\bar{\zeta}) = \prod_{m=1}^{k-1} \frac{\bar{\zeta} - \bar{\zeta}_{S_m}}{\bar{\zeta}_{S_k} - \bar{\zeta}_{S_m}} \prod_{m=k+1}^{n+2} \frac{\bar{\zeta} - \bar{\zeta}_{S_m}}{\bar{\zeta}_{S_k} - \bar{\zeta}_{S_m}} \quad (11)$$

are the $(n + 1)$ order Lagrange interpolation polynomials those can be integrated analytically:

$$I_k(\zeta) = \int_{-1}^{\zeta} P_k^{n+1}(\bar{\zeta}) d\bar{\zeta} \quad k = 1..n + 2 \quad (12)$$

So the integral with its interpolation:

$$\int_{-1}^{\zeta} f(\bar{\zeta}) d\bar{\zeta} \approx \int_{-1}^{\zeta} \sum_{k=1}^{n+2} f(\bar{\zeta}_{S_k}) P_k^{n+1}(\bar{\zeta}) d\bar{\zeta} = \sum_{k=1}^{n+2} f(\bar{\zeta}_{S_k}) I_k(\zeta) \quad (13)$$

4. QUASI 2D ELEMENT AND NUMERICAL INTEGRATION

Since the coordinate “ z ” has been transferred to a dimensionless “ ζ ” coordinate, and the $(0..h)$ range to $(-1..1)$, furthermore and the $h(x,y)$ gap size independent from z , only the contact area has to be divided into shapes characteristic of a particular 2D element type and then derived into a unified shape by means of conform transformation for numerical integration [4] in order to carry out the integrations.

$$\int_{A_c} f(x, y) dx dy = \sum_e \int_{A_c^e} f^e(x, y) dx dy = \sum_e \int_{-1}^1 \int_{-1}^1 f(x^e(\xi, \eta), y^e(\xi, \eta)) |\mathbf{J}| d\xi d\eta \quad (14)$$

Conform geometry transformation by Legendre shape functions (\mathbf{N}) according to [4] looks like:

$$x^e(\xi, \eta, t) = \sum_i X_i^e(t) N_{x_i}^e(\xi, \eta) = \mathbf{N}_x^{eT}(\xi, \eta) \mathbf{X}^e(t) \quad (15)$$

$$y^e(\xi, \eta, t) = \sum_j Y_j^e(t) N_{y_j}^e(\xi, \eta) = \mathbf{N}_y^{eT}(\xi, \eta) \mathbf{Y}^e(t) \quad (16)$$

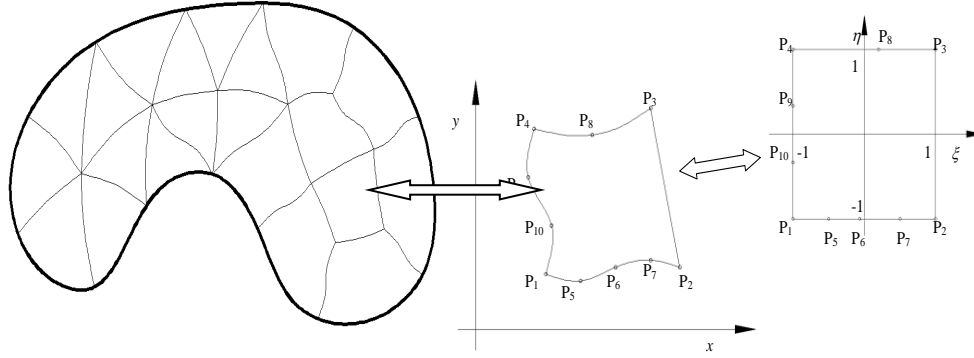


Figure 2. Mesh transformation

This integration is carried out in most cases numerically by means of Gaussian quadrature [4]:

$$\int_{-1}^1 \int_{-1}^1 f(\xi, \eta) |\mathbf{J}| d\xi d\eta = \sum_{i=1}^n \sum_{j=1}^m w_{G_i} w_{G_j} f(\xi_{G_i}, \eta_{G_j}) |\mathbf{J}(\xi_{G_i}, \eta_{G_j})| \quad (17)$$

Where ξ_G and η_G specified points within the domain of integration and w_G are weights at specified points [4].

Legendre shape functions (\mathbf{N}) according to [4] have been used for the polynomial approximation of the un-known variables. Only 2D approximation needed for the gap size, deformation and the pressure.

$$h_g^e(\xi, \eta, t) = \sum_k H_{g_k}^e(t) N_{h_k}^e(\xi, \eta) = \mathbf{N}_g^{eT}(\xi, \eta) \mathbf{H}_g^e(t) \quad (18)$$

$$\delta_s^e(\xi, \eta, t) = \sum_k H_{\delta_s k}^e(t) N_{h_k}^e(\xi, \eta) = \mathbf{N}_g^{eT}(\xi, \eta) \mathbf{H}_{\delta_s}^e(t) \quad s=1,2 \quad (19)$$

$$\mathbf{h}^e = \begin{bmatrix} \mathbf{N}_g^{eT}, 1 \\ \mathbf{H}_g^e + \mathbf{H}_{\delta_1}^e + \mathbf{H}_{\delta_2}^e \\ \Delta_{rigid} \end{bmatrix} = \mathbf{N}_h^{eT}(\xi, \eta) \mathbf{H}^e(t) \quad (20)$$

$$p^e(\xi, \eta, t) = \sum_l P_l^e(t) N_{p_l}^e(\xi, \eta) = \mathbf{N}_p^{eT}(\xi, \eta) \mathbf{P}^e(t) \quad (21)$$

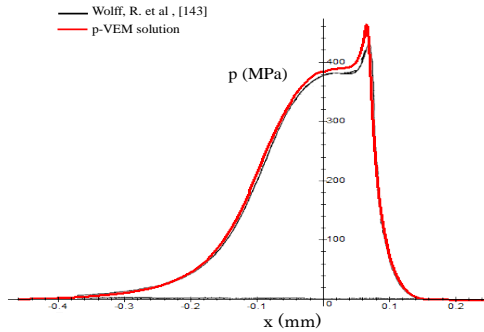


Figure 3. Pressure distribution for pure rolling

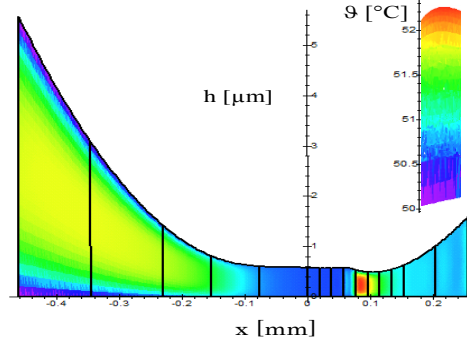


Figure 4. Temperature distribution for pure rolling

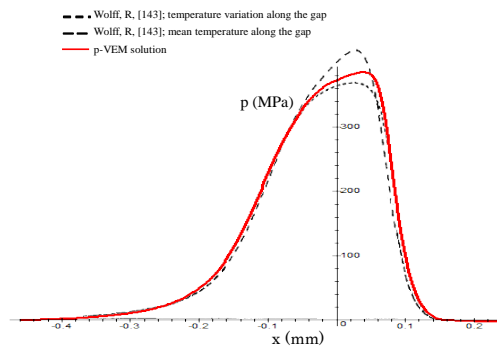


Figure 5. Pressure distribution with $S = 1.9$

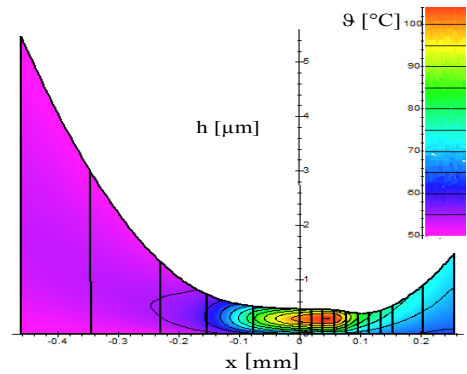


Figure 6. Temperature distribution with $S = 1.9$

The calculations were carried out for the state of pure rolling contact and with 1.9 sliding ratio. The elasto-hydrodynamic problem was solved with the use of the optimized Newton-Raphson method [3] and the thermodynamical problem by the attenuated direct algorithm in iterative manner. The pressure distribution obtained is shown in *Figure 3* and *Figure 5*. The gap size formed as well as the temperature distribution in *Figure 4* and *Figure 6*.

6. IMPLEMENTATION OF EHD PROBLEM TO FEM SOFTWARE

The Comsol Multiphysics software was used for calculating EHD problems. The Comsol Multiphysics uses the finite element formulation with Lagrange test functions to solve numerical problems. The weak formulation of the hydrodynamic problem can be created in the Mathematics module and model can be freely modified. The elastic deformation of the surface and the rigid displacement of the surfaces can

be calculated in the Structural Mechanics module which uses the common structural finite element methods. Since optimized Newton-Rapshon method [3] cannot be adopt to Comsol Multiphysics the solution has been stabilized be Streamline-up-wind/Petrov-Galjorkin and isotropic diffusion method. The results can be seen in *Figure 7* and *Figure 8*.

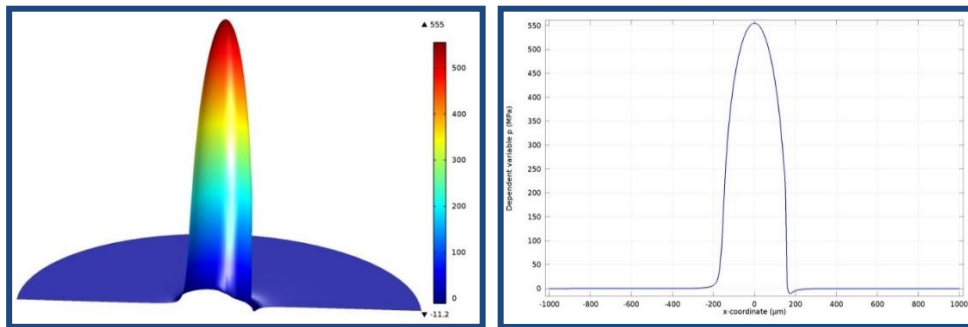


Figure 7. Pressure distribution of point contact

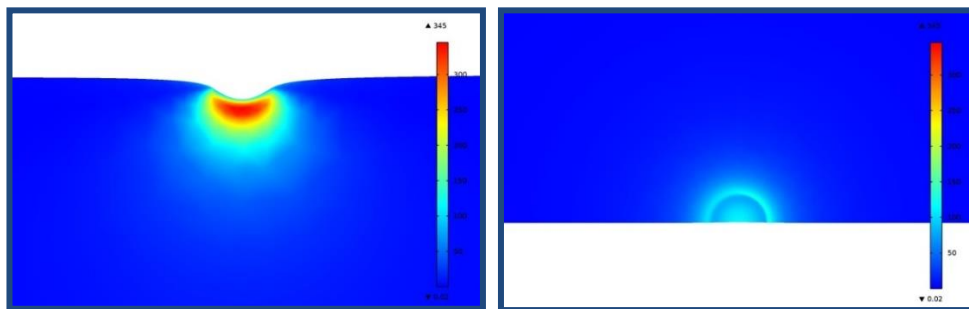


Figure 8. Surface deformation and subsurface stress distribution

7. CONCLUSION

For the three-dimensional contact problem of lubrication, a two-dimensional lubrication fluid film finite element was developed. A remarkable property of this element is that only a two-dimensional mesh has to be maintained. Furthermore, pressure and film thickness can be handled as independent element variables. Integration through the thickness is carried out by making use of dimensionless thickness coordinate. Three dimensional behaviour of the fluid film temperature can be modelled using higher order approximations through the thickness direction. The method has been verified by line contact and the EHD part has been already implemented to commercial FEM software. Implementation of the thermal part is under development.

ACKNOWLEDGEMENTS

The research was supported by the European Union and the State of Hungary, co-financed by the European Social Fund in the framework of TÁMOP-4.2.4.A/2-11/1-2012-0001 ‘National Excellence Program’ and National Research, Development and Innovation Office - NKFIH, K115701.

REFERENCES

- [1] Carslaw, H. S. & Jaeger, J. C. (1959). *Conduction of Heat in Solids*. Oxford University Press.
- [2] Johnson, K. L. (1987). *Contact Mechanics*. 2nd Ed., Cambridge Univ. Press.
- [3] Szávai, Sz. & Kovács, S. (2014). *P-version FEM model of TEHD lubrication and its implementation to study surface modified contact bodies behaviour*. BALKANTRIB'14: Proceedings, Sinaia, Romania, pp. 716–727.
- [4] Páczelt, I. (1999). *Finite Element Method in Engineering Practice I. Part (Végeselem-módszer a Mérnöki Gyakorlatban I. Kötet)*. Miskolc: Miskolci Egyetemi kiadó.
- [5] Wolff, R., Nonaka, T., Kubo, A. & Matsuo, K. (1992). Thermal Elastohydrodynamic Lubrication of Rolling/Sliding Line Contacts. *ASME J. of Tribology*, Vol. 114, No. 4, pp. 706–713.

METHODS FOR THE DETECTION AND ANALYSIS OF BEARING FAILURES

DÁNIEL TÓTH–ATTILA SZILÁGYI–GYÖRGY TAKÁCS

University of Miskolc, Department of Machine Tools
3515 Miskolc-Egyetemváros
toth.daniel@uni-miskolc.hu; szilagyi.attila@uni-miskolc.hu;
takacs.gyorgy@uni-miskolc.hu

Abstract: Bearings have a very important role in almost all rotating machine. Their operating properties impact the function of the whole machine. Failures of bearings can cause machine malfunction or even lead to catastrophic accidents. In order to prevent these events, continuous failure detection is necessary. This paper focuses on the methods for detection of bearing failures.

Keywords: bearing failures, analysis techniques, signal processing

1. INTRODUCTION

Bearings can be found extensively in domestic- and industrial applications. Their usage means risk for almost all forms of rotating equipment, such as pumps, machine tools, generators, electric motors, starters etc. These frequently used components have special importance in the course of investigations because their failure can cause big damages. The success of bearing life prediction depends on precise defect detection.

2. BEARING FAILURES

Even if bearings are being used under excellent conditions, sooner or long after material fatigue will befall. Besides other things unfavourable operating environment, contaminated or peculiarly moist areas and improper handling practices induce premature failures. Commonly the service life of bearings is expressed either as a period of time or as the total number of rotations before the incidence of failures in the outer ring, inner ring or rolling element because of rolling fatigue, as a result of repeated stress. When bearing defect is found, even if it is insignificant, it is necessary to examine the phenomenon to determine causes. In this case not only the bearing but also the shaft, housing, and lubricant used with the bearing should be exhaustively investigated [1].

Every bearing failure creates its own characteristic damage. Defects can be divided into primary or secondary ones in many cases. Primary defects are for example the smearing, wear, corrosion, indentations, surface distress and the passage of electric current. Even these defects may lead to scrapping the bearings in consequence of noise, low efficiency, vibration and so forth. Secondary failures such as flaking

and cracks are rooted in primary ones. A wrong bearing generally indicates a combination of secondary and primary failure [2]. *Table 1* contains the most common bearing failures and parts in which they occur.

Table 1
Often occurring bearing damages [1]

<i>Bearing failure</i>	Bearing ring, Rolling element			Bearing ring	Cage	
	<i>·Raceway surface</i> <i>·Rolling surface</i>	<i>·Roller guide surface</i> <i>·Cage guide surface</i> <i>·Roller end face</i>	<i>·Others</i>	<i>·Fitting surface</i>	<i>·Pocket surface</i> <i>·Guide surface</i>	<i>·Rivet</i>
Smearing	□	□	–	–	–	–
Wear	□	□	□	□	□	×
Corrosion	□	□	□	□	□	□
Fretting	□	–	–	□	–	–
Cracks	×	×	×	×	×	×
Chips	×	×	□	×	×	×
Brinelling	□	□	□	□	–	–
Nicks	□	□	□	□	□	□
Flaking	×	–	–	–	–	–
Scratches	□	□	□	□	□	□
Scuffing	□	□	□	□	–	–
Seizure	×	×	×	×	×	–
Rust	□	□	□	□	□	□
Pear skin	□	–	–	–	–	–
Creep	–	–	–	□	–	–
Electric pitting	□	□	–	–	□	–
Failure of cage	–	–	–	–	□	×

Where × means that in principle, not reusable; □ signifies that reusable in accordance with seriousness of failure, by repairing or meeting required conditions; – means that no failure of this part [1].

The aforementioned failures eventually will be resulted in the endurance of the surface. Nevertheless, the total lifetime of a bearing is meant to be the number of revolution until the first indication of the surface endurance appears. If investigate some similar bearing under the same condition, it is apparent, that the obtained lifetimes may diverge. The one most common bearing failure is the outer ring defects,

whereas in most cases the outer ring comprises and the load invariably affects the same point of the outer ring through on the rollers.

3. ANALYSIS METHODS

Condition monitoring is one possibility of preventive maintenance program. The collected data can be used to locate machinery problems and corrective activities can then be implemented. Different techniques are used for the perception of bearing condition. Such methods are noise analysis, acoustic measurements, temperature monitoring, wear debris detection, vibration analysis etc.

3.1. Temperature monitoring

Bearing distributed defects generate excessive heat in the rotating parts. Bearing manufacturers have long been aware of the connection of heat to bearing life and have designed formulas to accurately calculate safe operating temperatures. The results indicate a temperature band in which both lubricants and bearings will operate at top performance with the least stress. As soon as outside the optimal temperature range, they will degrade at an accelerated rate. *Figure 1* shows the temperature range of a typical rolling element bearing. The red zone (No. 3) represents the critical section, the yellow zone (No. 2) symbolizes the decreasing lubricant and bearing life, the green zone (No. 1) expresses the optimal place for bearing and lubrication temperature [3].

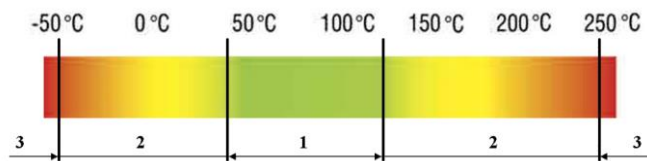


Figure 1. Thermal ranges [3]

Exist several temperature bands for distinct combinations of bearing and lubricant, but they will have the identical general trend regarding the optimal operating temperature and its effect on accelerated failure and wear. Thermal imaging empowers real-time temperature monitoring and localization of temperature increases. Moreover, it allows a spatial visualization of heat propagation in monitored areas [4].

3.2. Wear debris detection

The wear progress of a machine is commonly the result of many distinct, simultaneous wear mechanisms, each of which has its own way of affecting to the machine's operating environment and the changes that occur in it. If the poor operating conditions persist, the wear could either inflict parts of the machine to break or disturb the machine's operation. To allow detection at an untimely phase and control of the wear process, the size, amount and appearance of wear debris particles in the machine's

lubricating oil must be monitored [5]. In this method, the presence of metallic particles in the lubricant is detected by sensitive sensors. Furthermore, the spectrographic analysis of the dissimilar metallic elements in the lubricant could facilitate the location of the defect [6].

3.3. Acoustic measurement

Acoustic measurement is receiving increasing significance in condition monitoring of bearings. The most efficient acoustic-based bearing health monitoring is acoustic emission. This is a transient impulse generated by the rapid release of strain energy in solid material under mechanical or thermal stress. The perception of cracks is the main application of acoustic emission. Therefore, this method can be used as a device for condition monitoring of bearing failures and shaft cracks. The acoustic emission is not disturbed or influenced by other mechanical defects and noise in rotating machinery, such as unbalance and misalignment, which cannot be eliminated entirely and lightly. So the acoustic emission based methods are superior in certain areas, especially for early fault detection in bearings. The acoustic emission progress is capable of detecting defects forming deep inside the material, even before it would propagate out to the surface. The measurement of a machine's sound can also be employed for diagnosing damages in bearings. Usually, the precision of these methods depends on sound intensity data and sound pressure [7].

3.4. Noise analysis

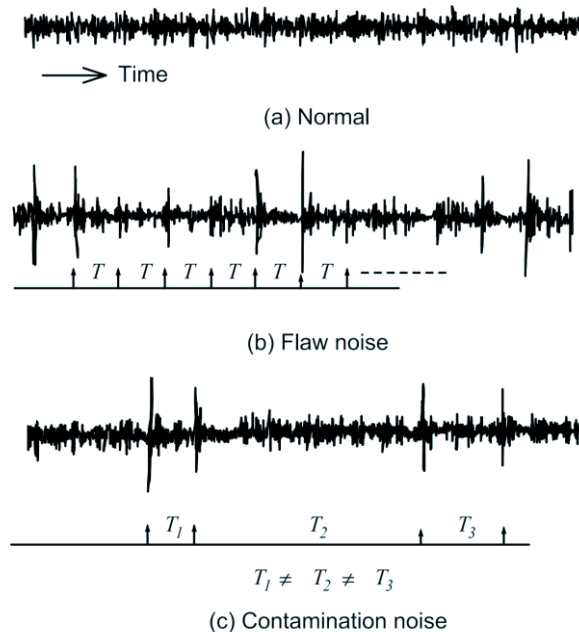


Figure 2. Waveform of noise due to contamination and flaw [8]

Even though the most modern manufacturing technology is used, sound still befall obviously in bearings. As the noise emitted by bearings is composed of all types of faults developed during the working time of the bearings and the manufacturing process, the effective values of certain noise quantities enable precise and quick examination [8]. Flaw noise has unique generation cycles or intervals if compared to other types of noise (*Figure 2*).

3.5. Vibration analysis

Vibration signals collected from bearings have affluent information on machine health conditions. Since the irregular vibration of rotary machines is the first sensory effect of rotary component failure, vibration analysis is widely spread in the industry. Vibration analysis can be applied for the diagnosis of almost every type of faults even localized or distributed. These methods benefits are accurate results, specific information and low-cost sensors. Several vibration analysis techniques available to analyse the bearing vibrations. Condition monitoring using vibration measurement can be classified into frequency domain, time domain, time-frequency domain and other techniques. The time-domain features are got from the raw vibration signal through the statistical parameters. Many stochastic indexes (like skewness, RMS value, peak-to-peak value, kurtosis etc.) use to characterize the status of bearings. Generally, the indexes of a damaged bearing tend to be bigger than the values of a normal bearing [9].

Frequency domain techniques are one of the most effective approach for the interpretation of bearing failures. The frequency domain involves to parse or display of vibration data based on the frequency. One main advantage of the method is that the repetitive nature of the vibration signals is exactly displayed as peaks in the frequency spectrum at the frequency where the repetition takes place. Time domain vibration signals are processed into the frequency domain by the adaptation of Fourier transform, typically in the shape of fast Fourier transform (FFT) algorithm. FFT is an algorithm to calculate the discrete Fourier transform and its inverse [6]. In a frequency spectrum (*Figure 3*) the horizontal axis is generally the frequency and the vertical axis is the amplitude of displacement, velocity or acceleration.

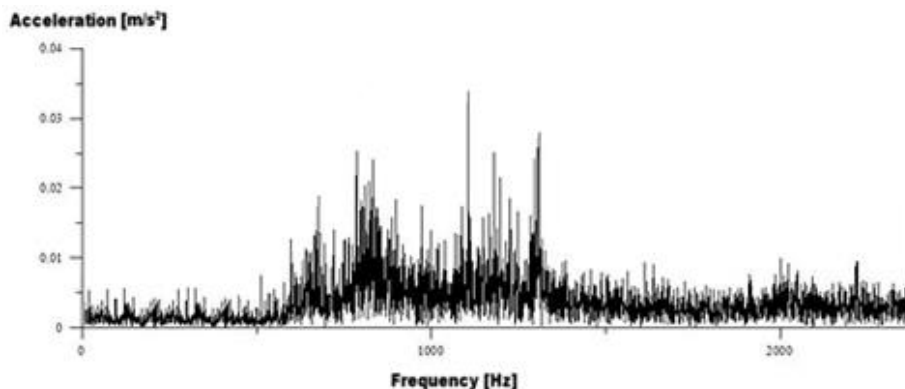


Figure 3. Frequency spectrum

Time–frequency domain analysis can manifest the signal frequency components, identifies their time variant features. These techniques have facility to handle both, stationary and non-stationary vibration signals. This is the one serious advantage over frequency domain techniques [10].

4. CONCLUSION

Many different methods have been evolved for monitoring and diagnosing of bearings in the past decades. Vibration based monitoring methods are advantageous tools in the field of predictive maintenance and efficacious in detecting defects in the bearings. Acoustic emission is receiving increasing attention as a complementary method for condition monitoring of bearings, as acoustic emission is enough sensitive to initial defects. Temperature monitoring of bearing is an effective method for fault perception in rotating machines.

ACKNOWLEDGEMENT

This research was supported by the ÚNKP-18-3 New National Excellence Program of the Ministry of Human Capacities.



REFERENCES

- [1] Koyo: Ball & Roller Bearings: *Failures, Causes and Countermeasures*. JTEKT Corporation, CAT.NO.B3001E.
- [2] SKF: *Bearing failures and their causes*, Product information 401.
- [3] Eugene Matzan (2007). Detecting Premature Bearing Failure. *Machinery Lubrication magazine*.
- [4] R. Schulz, S. Verstockt, J. Vermeiren, M. Loccufier, K. Stockman & S. Van Hoecke (2014). *Thermal Imaging for Monitoring Rolling Element Bearings*. QIRT.
- [5] J. K. Halme (2002). *Condition Monitoring of Oil Lubricated Ball Bearing Using Wear Debris and Vibration Analysis*. 6th International Tribology Conference, Perth: Western Australia.
- [6] P. P. Kharche & S. V. Kshirsagar (2014). Review of Fault Detection in Rolling Element Bearing. *IJIRAE*, Vol. 1, Issue 5.
- [7] Yongyong He, Xinming Zhang & Michael I. Friswell (2009). Defect diagnosis for rolling element bearings using acoustic emission. *Journal of Vibration and Acoustics*.
- [8] Tatsunobu Momono & Banda Noda (1999). Sound and Vibration in Rolling Bearings. *Motion & Control*, No. 6.

-
- [9] W. J. Staszewski & A. N. Robertson (2007). Time–frequency and time–scale analyses for structural health monitoring. *Philosophical Transactions: Mathematical, Physical and Engineering Sciences*, Vol. 365, No. 1851, Structural Health Monitoring.
 - [10] S. Patidar & P. K. Soni (2013). An Overview on Vibration Analysis Techniques for the Diagnosis of Rolling Element Bearing Faults. *IJETT*.

CURRENT DEVELOPMENT FOCUSES OF THE HYDROSTATIC BEARING DESIGN AND OPTIMIZATION

SÁNDOR GERGŐ TÓTH–ATTILA SZILÁGYI–GYÖRGY TAKÁCS

University of Miskolc, Department of Machine and Product Design
3515 Miskolc-Egyetemváros
szgttosg@uni-miskolc.hu
takacs.gyorgy@uni-miskolc.hu
szilagyi.attila@uni-miskolc.hu

Abstract: The number of scientific articles dealing with hydrostatic bearings has jumped significantly over the last decade due to the huge increase in the development of the Far East industry. With new numerical calculations and simulations, the shape of the bearing pads, the fluid film thickness can be optimized and the behaviour of special hydrostatic bearing designs can be tested. Considering the research results revealed, new directions for optimization, new applied fluids and further development directions are emerging.

Keywords: *hydrostatic bearings, hydrostatic guideways, Reynolds equation, optimization*

1. INTRODUCTION

Hydrostatic bearings could be one of the most important elements of machine tools due to their long service life and rotational precision, but their application is greatly hampered by their complex design, manufacturing precision sensitivity and the difficulty of describing their complicated mechanical properties compared to rolling bearings. For this reason, until the 1990s, the design of hydrostatic bearings was mostly based on previous measurements and experiences with analytical and numerical calculations. While hydrostatic bearing design companies in Europe are becoming increasingly obsessed, in the Far East, due to the large industrial developments, more and more publications are being dealt by developing hydrostatic bearings.

New publications – in the design and analysis of hydrostatic bearings – now consider engineering applicability. During the 1990–2018 period nearly 200 new publications were published on this topic. Some of the theoretical research deals with the improvement of the Reynolds equation, while a larger proportion of publications can be categorized by the shape of the bearing recesses, the pressure control method and the bearing design.

2. NEW GOVERNING EQUATIONS FOR HYDROSTATIC BEARINGS ANALYSIS

For studying hydrostatic bearings, the Reynolds equation provides a suitable base equilibrium, which can be used to determine the pressure distribution in a thin fluid

flow, while for thermal analysis, the energy equation can be selected. By combining the energy equation and the Reynolds equation, M. Khlifi [1] dealt with (1),

$$u \frac{\partial T}{\partial x} + \left(v - u \frac{\partial h}{\partial x} - w \frac{\partial h}{\partial z} \right) \frac{\partial T}{\partial y} + w \frac{\partial T}{\partial z} = \frac{k_c}{\rho c_p} \frac{\partial^2 T}{\partial y^2} + \frac{\eta}{\rho c_p} \left(\left(\frac{\partial u}{\partial y} \right)^2 + \left(\frac{\partial w}{\partial z} \right)^2 \right) \quad (1)$$

in which u , v , w is the liquid velocity at x , y and z direction, T is the temperature of the fluid, η is dynamic viscosity, ρ is density, k_c is thermal conductivity, and c_p is specific heat (at given pressure). The Reynolds equation is a second order differential equation, which can be solved analytically solely for Newtonian liquids. Rheological and other non-Newtonian fluids' flow behaviour was described by E De la Guerra Ochoa [2], who used the Reynolds equation for non-Newtonian fluids, using Carreau's dynamic viscosity function (2),

$$\eta = \eta_0 \left(1 + \left(\frac{\tau}{G} \right)^2 \right)^{\left(\frac{1 - \left(\frac{1}{n} \right)}{2} \right)} \quad (2)$$

where η_0 is the dynamic viscosity at steady state, τ is fluid shear stress, G is the shear modulus of elasticity, n (0.2 ... 1) is the Carreau exponential ratio that characterizes the given non-Newtonian fluid. The Reynolds equation was written for all currently applied bearing pads. The analytical solution of the Reynolds equation can be used to express the effects of each bearing design parameters, but complex mathematical calculations and simplifications are required. Employing CFD software, specific engineering problems are easier to simulate, but the interpretation of new models is difficult, therefore most theoretical research is based on numerical computation.

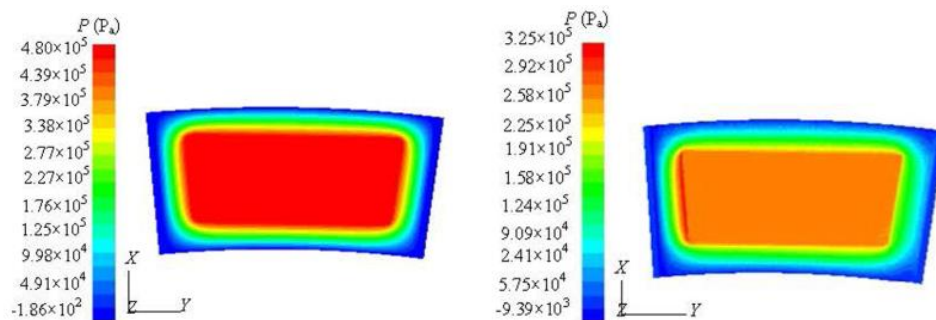


Figure 1. Fluid pressure distribution on a single pad bearing at different (2 and 20 1/min) rotational speed

Significantly fewer attempts were made to validate computational results and new models with experiments. Zhang Y. G. [3] verified the correlation between speed and pressure distribution by simulation with experimental and finite differential techniques.

3. RESEARCH RESULTS OF HYDROSTATIC THRUST BEARING

Hydrostatic thrust bearings generally are employed with a circular and annular bearing recesses. Due to circumferential geometry, the calculation of Reynolds equation can be made simpler with the cylinder coordinate system, and due to its lightweight manufacturability, most of the publication is concerned with this type of bearing. The publications are categorized into four theme groups: design and development of thrust bearings, surface texturing researches, bearing optimization, and studies about dynamic behaviour. Antoon van Beck [4] found that flexible bearing surfaces (*maintaining the thickness of the liquid film*) have a positive effect on the bearing load capacity. Moreover, the load capacity of the elastic support was derived analytically. Convex deformation should be avoided in this case, but a slight concave deformation is allowed. Later, the model was used by many studies in linear modelling and new numerical models that consider surface frictions too.

Y. Kang [5] investigated the dynamic behaviour of a rotational table supported by closed thrust bearings has been studied in the case of capillary compensation and constant oil pump. The stiffness of the hydrostatic thrust bearing regulated with the pump is much higher than for the capillary control. In addition, the static load significantly influences the dynamical characteristics of the hydrostatic bearing.

T. A. Osman [6] investigated the dynamics of axial hydrostatic bearing rings. Based on its calculations, an optimum flow rate can be determined for bearing load capacity, stiffness and damping. In addition, it can be stated that the bearing pad properties are greatly deteriorated if the bearing surfaces are not parallel to each other. F. Shen [7] studied multiple bearing recess shape (*rectangular, circular, ring, ellipse*), based on the results the highest stiffness can be achieved with the circular bearing recess, while the highest load capacity can be provided with the annular recess bearing.



Figure 2. Standing pad of hydrostatic thrust bearing allocated with optimized grooves

The centrifugal inertia force causes a high speed limit for hydrostatic thrust bearings. To compensate this effect, the spiral texturing of bearing surfaces is studied, and the applicability of streamlined bearing grooves [8] is examined. At present, these specially designed bearings are only employed for micro-manufacturing and aerostatic bearings.

4. RESEARCH RESULTS OF HYDROSTATIC JOURNAL BEARING

The number of publications about hydrostatic journal bearings is considerably lower than for thrust bearings, mainly due to the more complex bearing geometry. Most of the publications deal with the simulation of steady loads in bearings, with a smaller fraction of the description of dynamic behaviour, and the combination of journal-thrust bearings.

The utilizing of hydrostatic journal bearings is greatly influenced by their speed limitations. In the case of compressible liquids, the damping capabilities of the journal bearing decreases at low speeds, while at high speeds whirl instability appears [9]. S. C Jain compared the various recess pressure control methods with an analytical solution. Based on the calculations, the maximum permissible bearing loads and stiffness can be achieved by regulating the diaphragm flow control valve (*Figure 3*).

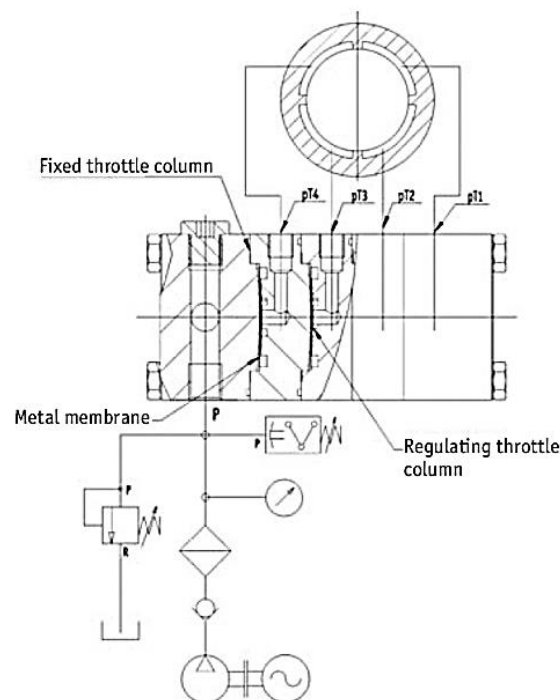


Figure 3. Hydraulic circuit diagram of the diaphragm constant flow valve (*Hyprostatik*)

Jerry C. T. Su and K. N. Lie [10] investigated hybrid (*hydrostatic/hydrodynamic*) bearing high-speed rotation phenomena. The rotation induces a hydrodynamic effect, the hydrostatic limit of the hydrostatic effect can be extended by several rows of grooved outlets, however, hydrodynamic stiffness deteriorates. The hydrodynamic effect can be improved by increasing the bearing length/diameter (L/D). In the case of high speed operation, it is advisable to construct smaller outlets. S. C. Sharma [11] examined different recess patterns according to selected bearing parameters. The rectangular recess provides the highest loadability depending on the thickness of the oil film. However, the highest bearings stiffness could be achieved with circular recess shape. The triangular recess shape can be used to stabilize for high speed operation. Parallel with these results, experiments with magnetorheological fluids (*containing nano-sized magnetic particles*) have also begun.

5. CURRENT RESEARCHES ABOUT HYDROSTATIC GUIDEWAYS

Among the hydrostatic bearings, the production of hydrostatic guideways is the simplest one because of the design of a regular bearing recess. The main directions of current research are the study and simulation of the dynamic behaviour of hydrostatic guideways, and the research of motion error analysis and optimization possibilities. Much less research has been done in the past on hydrostatic guideways, since the Reynolds equation in the Descartes coordinate system is more difficult to simplify, which complicates analytical computation.

Yikang D. U. [12] investigated the dynamic properties of the hydrostatic guideway systems, considering the fluid compressibility and inertia force, and based on the results, the Maxwell Dynamic Model can be used for liquid lubrication.

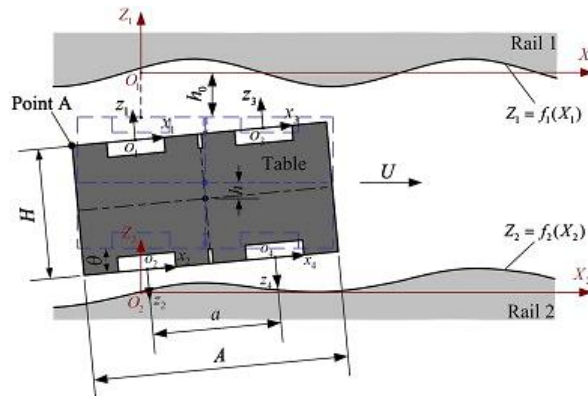


Figure 4. Theoretical model for determining the motion error of the hydrostatic guide [13]

Zhiwei Wang [13] created a new model for determining the motion of the hydrostatic guides (*Figure 4*). The speed of the table also affects the motion flow, and by increasing the feed pressure this effect can be reduced. By increasing the thickness of the liquid film, the movement error can be improved.

6. SUMMARY

The following article summarizes the major scientific publications on various hydrostatic bearings. Most publications still be based on the Reynolds equation that can be used to analyse liquid film on the surface of different types of bearings with good efficiency and accuracy but can only provide an approximate result for describing the flow in the bearing recesses. With the appearance of non-Newtonian fluids, the Reynolds equation also needs to be modified to handle changes in its dynamic viscosity.

The simplified analytical solution is computationally developed by numerical calculations. New, more accurate calculation models are laid down, which increasingly consider the relationship between bearing parameters. Due to the shortening of the calculation times and the increase in the calculation accuracy, simulations based on finite differential and finite element methods can be created within the CFD system.

The pressure regulation of the hydrostatic bearing recess can be accomplished by means of a capillary, orifice or a diaphragm flow control valve, with the latter being attained the highest loadability and stiffness at present. Although with the hydrostatic bearing self-regulating system (*servo valves*), it would be possible to achieve a constant, directly controlled pressure without pressure control elements. Magnetic rheological fluids could also be used to internal regulate by increasing bearing capacity.

Numerous researches deal with the optimization of the shape of the bearing plains and the recesses. The spiral grooves or streamlined bearing recesses are currently present only at hydrostatic thrust bearings. With CFD simulations, the recess shape can be optimized for hydrostatic journal bearings. With new optimization methods, bearing design and dimensioning can also be improved.

Employing hydrostatic guideway systems and bearings in Europe are increasingly peripheral and new research results are still expected from the Far East.

ACKNOWLEDGEMENT

The described article was carried out as part of the EFOP-3.6.1-16-00011 “Younger and Renewing University – Innovative Knowledge City – institutional development of the University of Miskolc aiming at intelligent specialisation” project implemented in the framework of the Szechenyi 2020 program. The realization of this project is supported by the European Union, co-financed by the European Social Fund.

REFERENCES

- [1] M. El Khlifi, D. Souchet, M. Hajjam & F. Bouyahia (2007). Numerical Modeling of Non-Newtonian Fluids in Slider Bearings and Channel Thermohydrodynamic Flow. *J. Tribol.*, T 129; pp. 695–699.
- [2] E. de la G. Ochoa, J. E. Otero, A. S. López & E. C. Tanarro (2015). Film thickness predictions for line contact using a new Reynolds–Carreau equation. *J. Tribol.*, 82, pp.133–141.

-
- [3] Zhang Y., Fan L., Li R., Dai C. & Yu X. (2013). Simulation and experimental analysis of supporting characteristics of multiple oil pad hydrostatic bearing disk. *Journal of Hydrodynamics*, 25 (2), pp. 236–241.
- [4] A. van Beek & R. A. J. van Ostayen (1994). Analytical solution for tilted hydrostatic multi-pad thrust bearings of infinite length. *Tribology International*, 30, pp. 33–39.
- [5] Y. Kang, H.-C. Chou, Y.-P. Wang & C. H. Chen (2013). Dynamic Behaviors of a Circular Worktable Mounted on Closed-Type Hydrostatic Thrust Bearing Compensated by Constant Compensations. *Journal of Mechanics*, 29, pp. 297–308.
- [6] T. A. Osman, Z. S. Safar & M. O. A. Mokhtar (1991). Design of annular recess hydrostatic thrust bearing under dynamic loading. *Trib. Internat.*, 24, pp.137–141.
- [7] F. Shen, C.-L. Chen & Z.-M. Liu (2014). Effect of Pocket Geometry on the Performance of a Circular Thrust Pad Hydrostatic Bearing in Machine Tools. *Trib. Transactions*, 57, pp.700–714.
- [8] M. Fesanghary & M. M. Khonsar (2013). On the optimum groove shapes for load-carrying capacity enhancement in parallel flat surface bearings: Theory and experiment. *Trib. Inter.*, 67 pp. 254–262.
- [9] W. B. Rowe (1980). Dynamic and Static Properties of Recessed Hydrostatic Journal Bearings by Small Displacement Analysis. *J. Lubrication Tech.*, 102, pp.71–79.
- [10] J. C. T. Su & K. N. Lie: Rotational effects on hybrid hydrostatic/hydrodynamic journal bearing. *Industral Lubr. and Trib.*, 53, No. 6, pp. 261–269.
- [11] S. C. Sharma, R. Sinhasan, S. C. Jain, N. Singh & S. K. Singh (1998). Performance of Hydrostatic/Hybrid Journal Bearings with Unconventional Recess Geometries. *J. Trib. Transactions*, 41, pp. 375–381.
- [12] Yikang, D., Kuanmin, M., Yaming, Z., Fengyun, W., Xiaobo, M. & Bin, L. (2015). Dynamic modeling of hydrostatic guideway considering compressibility and inertia effect. *Frontiers of Mechanical Engineering*, 10, pp.78–88.
- [13] Zhiwei, W., Wanhua, Z., Yaolong, C. & Bingheng, L. (2013). Prediction of the effect of speed on motion errors in hydrostatic guideways. *International J. Machine Tools & Manufacture*, 64, pp.78–84.

REVIEWING COMMITTEE

Á. DÖBRÖCZÖNI	Institute of Machine and Product Design University of Miskolc H-3515 Miskolc-Egyetemváros, Hungary machda@uni-miskolc.hu
F. J. SZABÓ	Institute of Machine- and Product Design University of Miskolc H-3515 Miskolc-Egyetemváros, Hungary machszf@uni-miskolc.hu
A. SZILÁGYI	Department of Machine Tools University of Miskolc H-3515 Miskolc-Egyetemváros, Hungary szilagyi.attila@uni-miskolc.hu
J. PÉTER	Institute of Machine and Product Design University of Miskolc H-3515 Miskolc-Egyetemváros, Hungary machpj@uni-miskolc.hu
GY. HEGEDŰS	Department of Machine Tools University of Miskolc H-3515 Miskolc-Egyetemváros, Hungary hegedus.gyorgy@uni-miskolc.hu
F. SARKA	Institute of Machine and Product Design University of Miskolc H-3515 Miskolc-Egyetemváros, Hungary machsf@uni-miskolc.hu
J. ERDÉLYI	Institute of Foundry University of Miskolc H-3515 Miskolc-Egyetemváros, Hungary janos.erdelyi@uni-miskolc.hu
J. SZENTE	Institute of Machine and Product Design University of Miskolc H-3515 Miskolc-Egyetemváros, Hungary machszj@uni-miskolc.hu

Secretariat of the Vice-Rector for Research and International Relations,
University of Miskolc,
Responsible for the Publication: Prof. dr. Tamás Kékesi
Published by the Miskolc University Press under leadership of Attila Szendi
Responsible for duplication: Erzsébet Pásztor
Editor: Dr. Ágnes Takács
Number of copies printed:
Put the Press in 2018
Number of permission: TNRT–2018– 478 –ME
HU ISSN 1785-6892 in print
HU ISSN 2064-7522 online